PHYSICAL REVIEW D **89,** 054035 (2014)

Sivers function in the quasiclassical approximation

Yuri V. Kovchegov and Matthew D. Sievert

Department of Physics, The Ohio State University, Columbus, Ohio 43210, USA

(Received 4 November 2013; published 26 March 2014)

We calculate the Sivers function in semi-inclusive deep inelastic scattering (SIDIS) and in the Drell-Yan process (DY) by employing the quasiclassical Glauber-Mueller/McLerran-Venugopalan approximation. Modeling the hadron as a large "nucleus" with nonzero orbital angular momentum (OAM), we find that its Sivers function receives two dominant contributions: one contribution is due to the OAM, while another one is due to the local Sivers function density in the nucleus. While the latter mechanism, being due to the "lensing" interactions, dominates at large transverse momentum of the produced hadron in SIDIS or of the dilepton pair in DY, the former (OAM) mechanism is leading in saturation power counting and dominates when the above transverse momenta become of the order of the saturation scale. We show that the OAM channel allows for a particularly simple and intuitive interpretation of the celebrated sign flip between the Sivers functions in SIDIS and DY.

DOI: 10.1103/PhysRevD.89.054035 PACS numbers: 12.38.Bx, 12.38.Cy, 13.88.+e, 24.85.+p

I. INTRODUCTION

Single transverse spin asymmetries (STSAs) generated in semi-inclusive deep inelastic scattering (SIDIS) and in hadronic collisions are one of the hot topics of research in quantum chromodynamics (QCD), promising unparalleled insight in the physics of chiral symmetry breaking and quark confinement. In the factorization framework involving transverse momentum-dependent distribution functions (TMDs) [1,2], the origin of STSAs is chiefly ascribed either to the quark TMDs (Sivers effect [3,4]), to multiple partonic rescattering [5–14], or to the quark fragmentation functions (Collins effect [15]).

While both the quark TMD and the fragmentation function are nonperturbative, and, according to the conventional wisdom, cannot be calculated form first principles, it is desirable to understand the detailed physical mechanism leading to generation of STSAs in QCD. To that end, significant progress has been achieved by Brodsky, Hwang, and Schmidt (BHS) in Ref. [10] (see also Refs. [5–7,9,11,16,17]), where, in a quark-diquark proton model calculation, it has been shown that the STSA in SIDIS can be generated through an interference of the final-state parton rescattering diagram with the Born-level amplitude. In essence, it was shown in Refs. [10,11] that multiple partonic rescatterings are key to generating the asymmetry. The multiple rescatterings are often referred to as the "lensing" interaction, since, in SIDIS, the associated color-Lorentz force tries to attract the knocked-out quarks back into the hadron [18,19], thus "focusing" them. The effects of such multiple rescatterings can be absorbed into the Sivers distribution function of a polarized hadron in SIDIS [11,20].

A consequence of this understanding of the origin of STSA in SIDIS is that the Sivers function (and hence, the asymmetry itself) has to change sign between SIDIS and the Drell-Yan process (DY). At the level of the operator matrix element, this conclusion has been reached in Ref. [11], while an illustration of this result in the BHS model was completed only recently [21] (see also Ref. [22] for the outline of the calculation). It is our understanding that in the "lensing" interpretation of STSAs, this sign change corresponds to the color-Lorentz force changing sign from attractive to repulsive between a knocked-out quark in SIDIS and the incoming antiquark in DY.

The goal of the present work is to extend our understanding of the physical mechanism behind the STSA beyond the quark-diquark model of the proton used in Refs. [10,21,22] (see Refs. [23,24] for other efforts in a similar direction). In particular, multiple partonic rescatterings in high-energy scattering can be particularly simply accounted for in the framework of the quasiclassical approximation to QCD employed in the Glauber-Mueller (GM) [25] and, equivalently, McLerran-Venugopalan (MV) [26–28] models. In these approaches the hadron is modeled by a large nucleus, with a large number A of nucleons in it. The large number of nucleons leads to a high density of small-x gluons in the nuclear wave function, which, in turn, generates a hard scale $Q_s \gg \Lambda_{\mathrm{QCD}}$ known as the parton saturation scale, justifying the use of perturbative QCD calculations. [For reviews of the saturation/color glass condensate (CGC) physics, see Refs. [29–33].] The fact that the quasiclassical approximation generates a hard scale justifying the approach indicates that it is not simply a "model" of QCD, but in fact, it represents a limiting behavior of strong interactions at high energy. Multiple rescatterings can be resummed in the GM/MV model as an expansion in powers of the parameter $\alpha_s^2 A^{1/3}$ [34]: the presence of a resummation parameter allows for a controlled approximation to the problem at hand. In the past, there were a number of efforts to include spin effects in the saturation/CGC framework [17,35–41].

To alleviate the worry about whether a large nucleus can adequately represent a proton (or any other hadron) in SIDIS and DY experiments, let us point out that in unpolarized scattering the proton may have a significant number of nonperturbatively generated large-x ($x > 0.01$) partons, which are modeled by "nucleons" in this large-nucleus approximation. The large-x partons/"nucleons," in turn, give rise to small-x gluons. The resulting expressions for the deep inelastic scattering (DIS) structure functions have been quite successful in describing HERA low-x data [42–45], also indicating relevance of the large-"nucleus" approximation to the proton wave function at small x.

In what follows, we would have to slightly modify the original MV model of the nucleus by giving the "nucleus" both a nonzero spin and a nonzero orbital angular momentum (OAM). Here this would mean that free nucleons in an approximately spherical bag, as considered originally in Refs. [26–28], would now be polarized and would be orbiting the nuclear spin axis. In a realistic polarized nucleus, the nucleons tend to form pairs with zero net OAM, such that the net spin of the nucleus is carried by the few unpaired nucleons and does not get very large (does not grow directly with A). Since it is not clear whether such effect (at the level of quarks and gluons) takes place in the proton we are trying to model, we will not make any particular assumptions about the polarizations and OAMs of the nucleons in our "nucleus."

The main physical mechanism for generating STSA in the quasiclassical framework is as follows: Imagine a large spinning nucleus. The nucleus is so large that it is almost completely opaque to a colored probe. This strong nuclear shadowing is due to multiple rescatterings in the nucleus generating a short mean free path for the quark, antiquark, or a gluon.

Let us first consider the Drell-Yan process on such a rotating nucleus with shadowing, as shown in Fig. 1 in the nuclear rest frame with the rotation axis of the nucleus perpendicular to the collision axis. The incoming antiquark (generated in the wave function of the other hadron) scatters on the "front" surface of the polarized nucleus due to the strong shadowing. Since the antiquark interacts with the nucleons, which, at the "front" of the nucleus, preferentially rotate with the nucleus out of the plane of the page in Fig. 1, the produced timelike virtual photons are produced preferentially out of the page, generating left-of-polarized-beam single spin asymmetry.[1]

The same mechanism can be applied to generate STSA in SIDIS, as illustrated in Fig. 2, also in the rest frame of

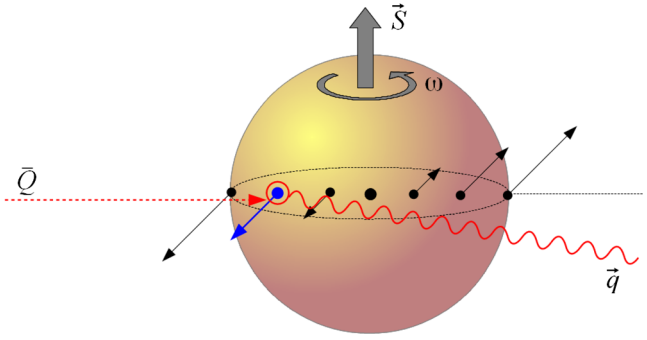

FIG. 1 (color online). The physical mechanism of STSA in DY as envisioned in the text.

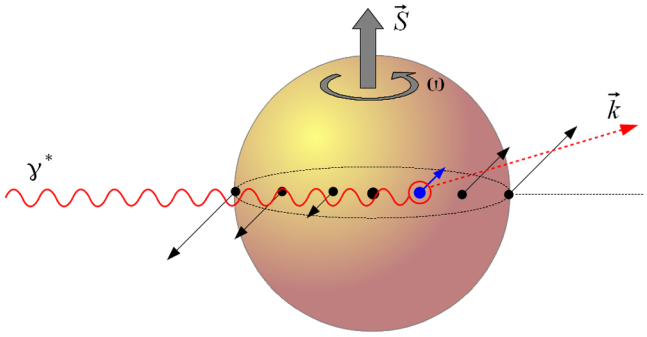

FIG. 2 (color online). The physical mechanism of STSA in SIDIS as envisioned in the text.

the nucleus. Now the incoming virtual photon interacts with the transversely polarized nucleus, producing a quark. For the quark to escape out of the nucleus and be produced, the interaction has to take place at the "back" of the nucleus, to minimize the path the quark needs to travel through the nucleus, maximizing its chances to escape. The nucleons in the "back" of the nucleus rotate preferentially into the page of Fig. 2: scattering of a virtual photon on such nucleons results in right-of-beam single spin asymmetry for the outgoing quarks (quarks produced preferentially with transverse momentum pointing into the page).

Spin asymmetries in DY and SIDIS shown in Figs. 1 and 2 are generated through a combination of OAM effects and nuclear shadowing. The two asymmetries are opposite in sign (left and right of beam) and, assuming that scattering in the two processes happens at equal distances from the nuclear edge, are likely to be equal in magnitude, in agreement with the prediction of Refs. [11,22].

As we will see below in the actual calculations, the STSAs in Figs. 1 and 2 do require multiple rescatterings, but they are needed solely to generate nuclear shadowing. Thus, the physical mechanism of Figs. 1 and 2 is quite different from the "lensing" interaction [10,22], in which the knocked-out quark in SIDIS "feels" the net color charge of the remainder of the proton and is attracted back by this

[1]This mechanism is similar in spirit to the original way of thinking by D. Sivers about the single transverse spin asymmetry (D. Sivers to M. Sievert, private communications). A heuristic classical picture of a polarized hadron or nucleus was pioneered in Ref. [46].

charge [18,19].[2] In the presence of shadowing, it would be much harder for the quark in SIDIS to "see" the whole remainder of the polarized proton (nucleus) coherently: thus, one expects the "lensing" effect to weaken with increasing shadowing (if we could increase shadowing without modifying the degree of the polarization of the nucleus). This is qualitatively different from the mechanism in Figs. 1 and 2, in which the asymmetry actually increases with shadowing. Clearly, the more opaque the nucleus is, the more likely the interactions to happen at its "front" in DY and at its "back" in SIDIS, making the asymmetry larger.

In the paper below, we will outline the calculations leading to the physical picture presented in Figs. 1 and 2. After some generalities in Sec. II, we proceed in Sec. III with the quasiclassical analysis of STSA in SIDIS. As mentioned above, to model the OAM of a polarized nucleus we have to assume that the nucleus is rotating. This implies a generalization of the original MV and GM models, in which nucleons are static, to include rotational motion of the nucleons. Hence, the nucleons need to have both well-defined positions and momenta: this is only possible in the classical limit. The classical MV model limit is achieved in Sec. III using the Wigner functions approach, which allows us to specify both the positions and momenta of the nucleons in the polarized nucleus.

We then proceed to the calculation of STSA in SIDIS, identifying two mechanisms for STSA generation: one is due to the coupling of the produced quarks' transverse momentum to the OAM of the nucleus, while another one is due to the STSA generated in the scattering of the virtual photon on an individual nucleon along the lines of the BHS mechanism [10] (Sivers function density). The former mechanism is leading in the saturation framework, being dominant in the saturation power counting (for nonzero OAM): it is order 1 for $\alpha_s^2 A^{1/3} \sim 1$. The latter mechanism is order α_s for $\alpha_s^2 A^{1/3} \sim 1$, and is thus subleading.

At large values of the produced quark transverse momentum k_T, the OAM mechanism gives the contribution to the Sivers function of the order $A\alpha_s m_N p_T Q_s^2/k_T^6$, with p_T the typical transverse momentum of the valence quarks in the polarized nucleus due to orbital motion and m_N the nucleon mass (with $m_N/3$ roughly the constituent quark mass), while the Sivers function density gives a contribution proportional to $A\alpha_s^2 m_N^2/k_T^4$. Assuming that $p_T \approx m_N$, we see that the Sivers function density mechanism dominates for $k_T > Q_s/\sqrt{\alpha_s}$; conversely, the OAM mechanism is dominant for $k_T < Q_s/\sqrt{\alpha_s}$, the domain including everything inside of the saturation region and a phase-space sector outside of that region.

A similar quasiclassical STSA calculation is carried out for the Drell-Yan process in Sec. IV, where we also explicitly show the mechanism for the sign reversal of the Sivers function outlined in this Introduction. We conclude in Sec. V by summarizing our results and outlining possible improvements of our results left for the future work.

II. DEFINITIONS: SINGLE SPIN ASYMMETRIES, SIVERS FUNCTION

The single transverse spin asymmetry is defined as

$$A_N(\underline{k}) \equiv \frac{\frac{d\sigma^\uparrow}{d^2kdy} - \frac{d\sigma^\downarrow}{d^2kdy}}{\frac{d\sigma^\uparrow}{d^2kdy} + \frac{d\sigma^\downarrow}{d^2kdy}} = \frac{\frac{d\sigma^\uparrow}{d^2kdy}(\underline{k}) - \frac{d\sigma^\uparrow}{d^2kdy}(-\underline{k})}{\frac{d\sigma^\uparrow}{d^2kdy}(\underline{k}) + \frac{d\sigma^\uparrow}{d^2kdy}(-\underline{k})} \tag{1}$$

for producing a hadron with transverse momentum $\underline{k}$ in SIDIS on a transversely polarized target and in polarized proton-proton collisions or a dilepton pair with transverse momentum $\underline{k}$ in the DY process on a polarized proton. The asymmetry A_N singles out a part of the production cross section proportional to $(\vec{S} \times \vec{p}) \cdot \vec{k}$, where $\vec{p}$ is the three-momentum of the polarized hadron pointing along the collision axis.

Throughout this paper, we will use light-cone coordinates $p^\pm \equiv p^0 \pm p^3$ with the corresponding metric $p \cdot q = \frac{1}{2} p^+ q^- + \frac{1}{2} p^- q^+ - \underline{p} \cdot \underline{q}$. Accordingly, we denote four-vectors as $p^\mu = (p^+, p^-, \underline{p})$, with the transverse momentum $\underline{p} \equiv (p^1, p^2)$ and $p_T = p_\perp = |\underline{p}|$.

As we have outlined above, a possible physical explanation of the asymmetry is the Sivers effect [3,4]. The aim of this work is to calculate the Sivers function in the quasiclassical approximation. To define the Sivers function, first consider a quark-quark correlation function in a polarized hadron or nucleus defined by [47,48]

$$\Phi_{ij}(x, \underline{k}; P, S) \equiv \int \frac{dx^- d^2x_\perp}{2(2\pi)^3} e^{i(\frac{1}{2}xP^+x^- - \underline{x}\cdot\underline{k})} \times \langle P, S|\bar{\psi}_j(0)\mathcal{U}\psi_i(x^+ = 0, x^-, \underline{x})|P, S\rangle, \tag{2}$$

where ψ_i is the quark field with Dirac index $i = 1, \ldots, 4$, while the quark is taken with transverse momentum $\underline{k}$ and the longitudinal momentum fraction x. The proton (or polarized nucleus) spin four-vector is S^μ, while $\mathcal{U}$ is the gauge link necessary to make the object on the right of Eq. (2) gauge invariant.

Below, when considering SIDIS and DY, we will work in the light-cone gauge of the projectile. Choosing the polarized proton (nucleus) to move along the light-cone x^+ direction, such that P^+ is large, we will work in the $A^- = 0$ gauge. In the quasiclassical approximation, the

[2] Applying this logic to DY, one would expect that to obtain a STSA sign reversal compared to SIDIS, one needs the antiquark in DY to "feel" an equal repulsive force from the rest of the proton (that is, from the proton without the quark which is about to annihilate the antiquark): however, it is unclear to us how the incoming antiquark can "feel" the force of only a part of the intact proton (excluding the quark) while interacting with the whole proton coherently.

$A^- = 0$ gluon field of a large ultrarelativistic nucleus moving along the x^+ direction has zero transverse component, $\underline{A} = 0$, such that the only nonzero component is A^+. Defining the Wilson line

$$V_{\underline{x}}[b^-, a^-] \equiv \mathcal{P} \exp\left[\frac{ig}{2}\int_{a^-}^{b^-} dx^- A^+(x^+ = 0, x^-, \underline{x})\right], \quad (3)$$

we write for the case of SIDIS [11,20]

$$\mathcal{U}^{\mathrm{SIDIS}} = V_{\underline{0}}^\dagger[+\infty, 0] V_{\underline{x}}[+\infty, x^-], \quad (4)$$

while for DY we have

$$\mathcal{U}^{\mathrm{DY}} = V_{\underline{0}}[0, -\infty] V_{\underline{x}}^\dagger[x^-, -\infty]. \quad (5)$$

In both cases we neglected the transverse gauge link at $x^- = \pm\infty$, since $\underline{A} = 0$ in the gauge we chose. As will become apparent below, the direction of the Wilson lines in the $\mathcal{U}$'s is given by the direction of motion of the outgoing quark in SIDIS and the incoming antiquark in DY. This results in different definitions of the correlator Φ_{ij} for the two processes, which is usually referred to as the controlled process dependence of the TMDs [11].

The correlation function Φ_{ij} is decomposed as [48,49]

$$\Phi_{ij}(x, \underline{k}; P, S) = \frac{M}{2P^+}\left[f_1(x, k_T)\frac{\not{P}}{M} + \frac{1}{M^2} f_{1T}^\perp(x, k_T)\epsilon_{\mu\nu\rho\sigma}\gamma^\mu P^\nu k_\perp^\rho S_\perp^\sigma - \frac{1}{M} g_{1s}(x, \underline{k})\not{P}\gamma^5 \right.$$
$$\left. - \frac{1}{M} h_{1T}(x, k_T) i\sigma_{\mu\nu}\gamma^5 S_\perp^\mu P^\nu - \frac{1}{M^2} h_{1s}^\perp(x, \underline{k}) i\sigma_{\mu\nu}\gamma^5 k_\perp^\mu P^\nu + h_1^\perp(x, k_T)\sigma_{\mu\nu}\frac{k_\perp^\mu P^\nu}{M^2}\right]_{ij}, \quad (6)$$

where M is the mass of the polarized proton or nucleus.

In the following, we will be using the Sivers function $f_{1T}^\perp(x, \underline{k})$ and the unpolarized quark TMD $f_1(x, \underline{k})$. These functions can be obtained from the correlator Φ_{ij} using the following expressions:

$$\Phi_{ij}(\gamma^+)_{ji}\big|_{\text{spin independent}} = 2f_1(x, k_T), \quad (7a)$$

$$\Phi_{ij}(\gamma^+)_{ji}\big|_{\text{spin dependent}} = \frac{2}{M}\epsilon^{ij} S_\perp^i k_\perp^j f_{1T}^\perp(x, k_T). \quad (7b)$$

III. SEMI-INCLUSIVE DEEP INELASTIC SCATTERING

We first consider the process of quark production in semi-inclusive deep inelastic lepton scattering on a transversely polarized heavy nucleus: $\ell + A^\uparrow \to \ell' + q + X$. The leptonic tensor can be factorized out in the usual way, so we represent the process as the scattering of a virtual photon: $\gamma^* + A^\uparrow \to q + X$. This photon carries a large spacelike virtuality $q_\mu q^\mu = -Q^2$ and knocks out a quark from one of the nucleons, which may then rescatter on the nuclear remnants. The nucleus is taken in the classical GM/MV approximation, which we augment by requiring that the nucleons be polarized and the nucleus rotate around the transverse spin axis, which leads to a nonzero OAM.

Consider first the lowest-order process shown in Fig. 3, in which a quark is ejected without rescattering.[3] We work in a frame (such as the photon-nucleus center-of-mass frame) in which the virtual photon moves along the x^- axis with a large momentum q^- and the nucleus moves along the x^+ axis with a large momentum P^+. In this frame, the kinematics are

$$P^\mu = \left(P^+, \frac{M_A^2}{P^+}, \underline{0}\right),$$
$$q^\mu = \left(-\frac{Q^2}{q^-}, q^-, \underline{0}\right),$$
$$p^\mu = \left(\alpha P^+, \frac{p_T^2 + m_N^2}{\alpha P^+}, \underline{p}\right),$$
$$k^\mu = \left(\frac{k_T^2}{k^-}, k^-, \underline{k}\right), \quad (8)$$

where M_A is the mass of the nucleus, and the on-mass-shell valence quark with momentum p^μ is a part of the light-cone

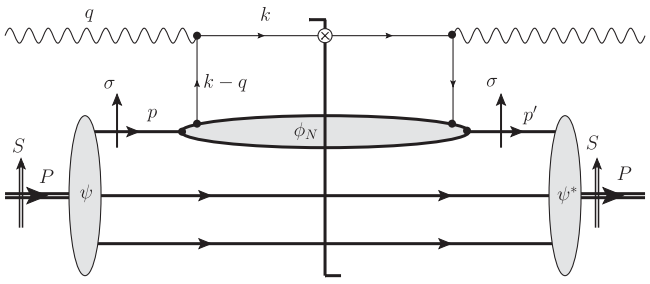

FIG. 3. The lowest-order SIDIS process in the usual α_s power counting. A quark is ejected from a nucleon in the nucleus by the high-virtuality photon, which escapes without rescattering. Different solid horizontal lines represent valence quarks from different nucleons in the nuclear wave function, with the latter denoted by the vertical shaded oval.

[3]In small-x physics, quark production is dominated by a higher-order-in-α_s process, where the virtual photon splits into a $q\bar{q}$ pair before hitting the target: since in this work $x = \mathcal{O}(1)$, the dipole process is not dominant, constituting an order-α_s correction to the channel shown in Fig. 3.

wave function of the nucleus. In what follows, we will model nucleons as made out of single valence quarks: in the end of the calculation, to go back to the nucleons, one simply would need to replace distribution functions in a valence quark with the distribution functions in the nucleons.

Let us denote the photon-nucleus center-of-mass energy squared by $s_A \equiv (P+q)^2$ and the photon-nucleon (valence quark) center-of-mass energy squared by $\hat{s} \equiv (p+q)^2$. We consider the kinematic limit $s_A \gg \hat{s}, Q^2 \gg p_T^2, k_T^2, M_A^2$ and work to leading order in the small kinematic quantities $\frac{\perp^2}{\hat{s}}, \frac{\perp^2}{Q^2}$, which we denote collectively as $\mathcal{O}(\frac{\perp^2}{Q^2})$. Since we are operating in the limit in which $Q^2 \gg \perp^2 \gg \Lambda^2$, the formalism of TMD factorization applies, justifying the use of the correlator [Eq. (2)] and decomposition [Eq. (6)]. Additionally, to a good accuracy one can assume that a typical scale for the momentum fraction α is $\mathcal{O}(1/A)$, where A is the mass number of the nucleus (in fact, $\alpha \approx 1/A$ for the single-valence quark "nucleons" at hand). In this limit,

$$p^+q^- = \hat{s} + Q^2,$$
$$q^+ = -\left(\frac{Q^2}{\hat{s}+Q^2}\right)p^+ = -xp^+ = -\alpha x P^+, \quad (9)$$

where $x \equiv Q^2/(2p\cdot q)$ is the Bjorken scaling variable per nucleon. The corresponding scaling variable for the entire nucleus is $x_A \equiv Q^2/(2P\cdot q) = \alpha x \approx x/A$. The kinematic limit at hand, $\hat{s} \sim Q^2 \gg p_T^2, k_T^2, M_A^2$, corresponds to $x \sim \mathcal{O}(1)$. The on-shell condition for the outgoing gluon is

$$k^- = \frac{k_T^2}{k^+} = q^- + \frac{p_T^2 + m_N^2}{\alpha P^+} - \frac{(\underline{p}-\underline{k})_T^2}{\alpha P^+ - \alpha x P^+ - k^+} \approx q^-, \quad (10)$$

which fixes the struck quark to be ejected along the x^- direction, so that its light cone plus momentum

$$k^+ = \frac{k_T^2}{q^-} = \left(\frac{k_T^2}{\hat{s}+Q^2}\right)p^+ = \left(\frac{k_T^2}{Q^2}\right)\alpha x P^+ \quad (11)$$

is small, since $\sqrt{\hat{s}} \sim Q \sim p^+ \gg k_T$. This also fixes the momentum fraction of the active quark just before interaction with the photon to be $x_F \equiv (k^+ - q^+)/p^+ \approx -q^+/p^+ = x$ in the usual way. (Note that $q^+ = -Q^2/q^- < 0$.)

In our frame, the x^- extent of the Lorentz-contracted nucleus is $L^- \sim \frac{M_A}{P^+}R$, where R is the radius of the nucleus in its rest frame. The incoming virtual photon and outgoing quark interact with the nucleus based on their corresponding coherence lengths: $\ell_\gamma^- \sim 1/|q^+|$ and $\ell_k^- \sim 1/k^+$, respectively. Comparing these to the size of the nucleus,

$$\frac{\ell_\gamma^-}{L^-} \sim \frac{1}{x}\frac{1}{\alpha M_A R} \sim \mathcal{O}(A^{-1/3}) \ll 1,$$
$$\frac{\ell_k^-}{L^-} \sim \frac{1}{x}\left(\frac{Q^2}{k_T^2}\right)\frac{1}{\alpha M_A R} \sim \mathcal{O}\left(\frac{Q^2+\hat{s}}{\perp^2}A^{-1/3}\right) \gg 1, \quad (12)$$

we see that the photon's coherence length is short, but the coherence length of the ejected quark is parametrically large for $\hat{s}, Q^2 \gg \perp^2 A^{1/3}$. Thus, for our calculation in which $x \sim \mathcal{O}(1)$, the virtual photon interacts incoherently (locally) on a single nucleon, but the ejected quark interacts coherently with all of the remaining nucleons it encounters before escaping the nucleus.

This limit thus combines the local "knockout" picture of the deep inelastic scattering process with the coherent rescattering that usually characterizes the small-x limit. In the formal limit of a large nucleus in which $\alpha_s \ll 1$ and $A \gg 1$ such that $\alpha_s^2 A^{1/3} \sim \mathcal{O}(1)$, these coherent interactions with subsequent nucleons must be resummed according to this saturation-based power counting.

A. Quark production in SIDIS

In general, it is rather straightforward to write an answer for the quasiclassical quark production in SIDIS. As we mentioned in the Introduction, here the problem is a little more subtle than usual, since we are interested in also including transverse and longitudinal motion of the nucleons in the nucleus in order to model its OAM. Thus, our quasiclassical description of the nucleus has to provide us with both the positions and momenta of the nucleons. This can be done using Wigner distributions.

Let us illustrate the method with a simple single scattering from Fig. 3. Just like in the parton model, the time scale of internucleon interactions is Lorentz-dilated in the infinite-momentum frame of the nucleus that we are working in. We can, therefore, write the scattering amplitude for the process in Fig. 3 as a product of the light-cone wave function ψ of the valence quarks in the nucleus (defined according to light-front perturbation theory rules [50,51] in the boost-invariant convention of Ref. [33]) with the quark–virtual photon scattering amplitude M_K:

$$M_{\rm tot} = \psi(p) M_K(p,q,k). \quad (13)$$

Here $\psi(p) = \psi(p^+/P^+, \underline{p})$ is the boost-invariant light-cone wave function of a valence quark (in one of the nucleons) in the nucleus, while M_K is the scattering amplitude for the "knockout" process $\gamma^* + q \to q + X$. The sum over valence quark spin and color is implied in Eq. (13). In calculating the quark production process we need to square this amplitude, we integrate it over the momentum of the final-state and sum over all nucleons in the nucleus. Since momenta k and q are fixed, this amounts to integrating over p. One gets

$$\int \frac{dp^+ d^2p}{2(p^+ + q^+)(2\pi)^3} |M_{\rm tot}|^2 = A \int \frac{dp^+ d^2p}{2(p^+ + q^+)(2\pi)^3} |\psi(p)|^2 \left| M_K(p,q,k) \right|^2. \quad (14)$$

First, let us introduce a Fourier transform of the valence quark wave function,

$$\psi(b) \equiv \psi(b^-, \underline{b}) = \int \frac{dp^+ d^2p}{2\sqrt{p^+}(2\pi)^3} e^{-ip\cdot b} \psi(p), \quad (15)$$

with $p \cdot b = \frac{1}{2} p^+ b^- - \underline{p} \cdot \underline{b}$. Next, we define the Wigner distribution for the valence quarks (which is closely related to the Wigner distribution of the nucleons in the quasiclassical MV model employed here) with the help of the Fourier transform [Eq. (15)]:

$$W(p,b) \equiv W(p^+, \underline{p}; b^-, \underline{b}) \equiv \int d^2\delta b d\delta b^- e^{ip\cdot\delta b} \psi\left(b + \frac{1}{2}\delta b\right) \psi^*\left(b - \frac{1}{2}\delta b\right). \quad (16)$$

Note that the wave function is normalized such that

$$\int \frac{dp^+ d^2p}{2p^+(2\pi)^3} |\psi(p)|^2 = 1, \quad (17)$$

giving

$$\int \frac{dp^+ d^2p db^- d^2b}{2(2\pi)^3} W(p,b) = 1. \quad (18)$$

Since

$$\int d^2b db^- W(p,b) = |\psi(p)|^2 / p^+, \quad (19)$$

we can recast Eq. (14) as

$$\int \frac{dp^+ d^2p}{2(p^+ + q^+)(2\pi)^3} |M_{\rm tot}|^2 = A \int \frac{dp^+ d^2p db^- d^2b}{2(2\pi)^3} \times W(p,b) \frac{p^+}{p^+ + q^+} |M_K(p,q,k)|^2. \quad (20)$$

Finally, in the following, as usual in the saturation framework, it would be convenient to calculate the scattering amplitude in (partial) transverse coordinate space. Writing

$$M_K(p,q,k) = \int d^2x e^{-i\underline{k}\cdot(\underline{x}-\underline{b})} M_K(p,q,\underline{x}-\underline{b}) \quad (21)$$

[with k^- and k^+ fixed by Eqs. (10) and (11)], we rewrite Eq. (20) as

$$\int \frac{dp^+ d^2p}{2(p^+ + q^+)(2\pi)^3} |M_{\rm tot}|^2 = A \int \frac{dp^+ d^2p db^- d^2b}{2(2\pi)^3} W(p,b) \frac{p^+}{p^+ + q^+} \times \int d^2x d^2y e^{-i\underline{k}\cdot(\underline{x}-\underline{y})} M_K(p,q,\underline{x}-\underline{b}) M_K^*(p,q,\underline{y}-\underline{b}). \quad (22)$$

Note that the Fourier transform in Eq. (21) appears to imply that $\underline{b}$ is the transverse position of one of the outgoing partons in Fig. 3, whereas in the Wigner distribution $\underline{b}$ is the position of the valence quark p. As we will shortly see, such interpretation is not inconsistent: in the classical limit of a large nucleus, the Wigner distribution is a slowly varying function of $\underline{b}$, with changes in W becoming significant over the variations of $\underline{b}$ over distances of the order of nucleon size 1 fm or larger. The valence quark and outgoing parton at $\underline{b}$ in Fig. 3 are perturbatively close to each other (being part of the same Feynman diagram), and hence the difference in their positions is outside the precision of $W(p,b)$ and can be taken to be the same in the Wigner distribution.

In Appendix A, we show that Eq. (22) holds not only at the lowest order, but when multiple rescatterings are included as well, such that in the kinematics outlined above

$$\int \frac{dp^+ d^2p}{2(p^+ + q^+)(2\pi)^3} |A_{\rm tot}|^2 = A \int \frac{dp^+ d^2p db^- d^2b}{2(2\pi)^3} W(p,b) \frac{p^+}{p^+ + q^+} \times \int d^2x d^2y e^{-i\underline{k}\cdot(\underline{x}-\underline{y})} A(p,q,\underline{x}-\underline{b}) A^*(p,q,\underline{y}-\underline{b}), \quad (23)$$

where we define the energy-independent (at the lowest nontrivial order) $2 \to 2$ scattering amplitudes by [see also Eqs. (A8) and (A11)] [33]

$$A(p,q,k) = \frac{M(p,q,k)}{2p^+ q^-}, \quad (24)$$

and $A(p,q,k)$ in Eq. (23) denotes the sum over rescatterings of the quark on any number of nucleons in the nucleus.[4] [Note that for a "nucleus" made out of a

[4]Strictly speaking, we need to include in Eq. (23) Wigner function convolutions with all the interacting nucleons in the nucleus: however, since in our kinematics only the first "knockout" process depends on the transverse momentum $p_\perp$ of the nucleon, we only keep one convolution with the Wigner function explicitly.

single nucleon, $p^+ = P^+$, which allows one to reduce Eq. (22) to Eq. (23) by neglecting the "spectator" nucleons.] We therefore conclude that the quark production cross section for the $\gamma^* + A \to q + X$ process can be written as

$$\frac{d\sigma^{\gamma^*+A\to q+X}}{d^2\mathrm{k}\mathrm{d}y} = A \int \frac{dp^+ d^2p db^- d^2b}{2(2\pi)^3} \times W(p,b) \frac{d\hat{\sigma}^{\gamma^*+NN\ldots N\to q+X}}{d^2\mathrm{k}\mathrm{d}y}, \quad (25)$$

where the cross section for producing a quark in γ^* scattering on the nucleons is

$$\frac{d\hat{\sigma}^{\gamma^*+NN\ldots N\to q+X}}{d^2\mathrm{k}\mathrm{d}y} = \mathcal{N} \int d^2x d^2y e^{-i\underline{k}\cdot(\underline{x}-\underline{y})} A_K(p,q,\underline{x}-\underline{b}) \times A_K^*(p,q,\underline{y}-\underline{b}) D_{\underline{x}\,\underline{y}}[+\infty, b^-], \quad (26)$$

with the semi-infinite fundamental dipole scattering amplitude given by [cf. Eq. (4)]

$$D_{\underline{x}\,\underline{y}}[+\infty, b^-] = \left\langle \frac{1}{N_c} \mathrm{Tr}[V_{\underline{x}}[+\infty, b^-] V_{\underline{y}}^\dagger[+\infty, b^-]] \right\rangle, \quad (27)$$

and with some $\hat{s}$ and Q^2-dependent prefactor $\mathcal{N}$. Here $y = \ln 1/x$ is the rapidity of the produced quark, and a factor of A in Eq. (25) accounts for the fact that the first scattering can take place on any of the A nucleons. We fixed the normalization of Eq. (25) by requiring it to be valid for a nucleus made out of a single nucleon, which would be described by a trivial Wigner distribution fixing the momentum and position of the nucleon by simple delta functions. (Alternatively one could require the formula to be valid for the case of a cross section $\hat{\sigma}$ independent of p and b.)

As already mentioned before, with the accuracy of the large-A classical approximation, the argument $\underline{b}$ in the Wigner distribution can be replaced by any other transverse coordinate involved in the scattering process. Hence, one can replace $\underline{b}$ in $W(b,p)$ from Eq. (25) with either $\underline{x}$ or $\underline{y}$ from Eq. (26), or with any linear combination of those variables. Replacing $\underline{b}$ in $W(b,p)$ from Eq. (25) with $(\underline{x}+\underline{y})/2$ and employing Eq. (26), we write

$$\frac{d\sigma^{\gamma^*+A\to q+X}}{d^2\mathrm{k}\mathrm{d}y} = A \int \frac{dp^+ d^2p db^-}{2(2\pi)^3} \times \int d^2x d^2y W\left(p, b^-, \frac{\underline{x}+\underline{y}}{2}\right) \times e^{-i\underline{k}\cdot(\underline{x}-\underline{y})} |A_K|^2(p,q,\underline{x}-\underline{y}) D_{\underline{x}\,\underline{y}}[+\infty, b^-], \quad (28)$$

where

$$|A_K|^2(p,q,\underline{x}-\underline{y}) \equiv \mathcal{N} \int d^2b A_K(p,q,\underline{x}-\underline{b}) A_K^*(p,q,\underline{y}-\underline{b}) = \int \frac{d^2k'}{(2\pi)^2} e^{i\underline{k}'\cdot(\underline{x}-\underline{y})} \frac{d\hat{\sigma}^{\gamma^*+N\to q+X}}{d^2k'dy}(p,q). \quad (29)$$

Substituting Eq. (29) into Eq. (28) yields

$$\frac{d\sigma^{\gamma^*+A\to q+X}}{d^2\mathrm{k}\mathrm{d}y} = A \int \frac{dp^+ d^2p db^-}{2(2\pi)^3} \times \int d^2x d^2y W\left(p, b^-, \frac{\underline{x}+\underline{y}}{2}\right) \times \int \frac{d^2k'}{(2\pi)^2} e^{-i(\underline{k}-\underline{k}')\cdot(\underline{x}-\underline{y})} \times \frac{d\hat{\sigma}^{\gamma^*+N\to q+X}}{d^2k'dy}(p,q) D_{\underline{x}\,\underline{y}}[+\infty, b^-]. \quad (30)$$

Equation (30) is our starting point for exploring the STSA in SIDIS: it gives the quark production cross section in the quasiclassical approximation.

The expression (30) is illustrated in Fig. 4: the first interaction between the incident virtual photon and a nucleon in the transversely polarized nucleus happens at the longitudinal coordinate b^-. A quark is knocked out, which proceeds to interact with the rest of the nucleons in the nucleus. This latter interaction is recoil-less and is encoded in a Wilson line.

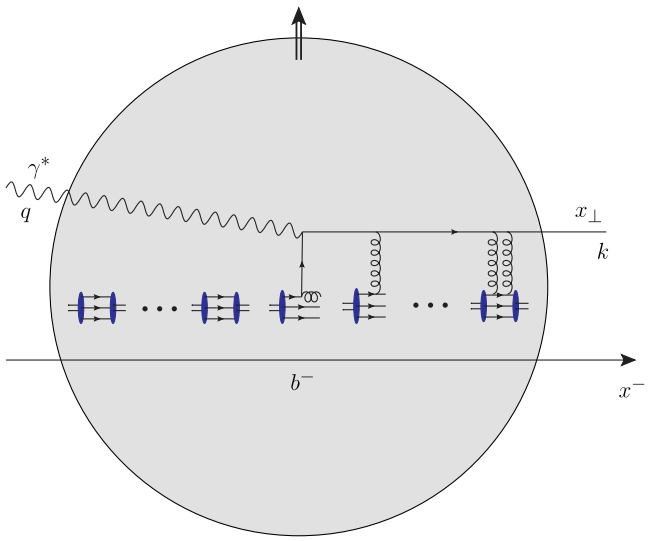

FIG. 4 (color online). Space-time structure of quark production in the quasiclassical SIDIS process in the rest frame of the nucleus, overlaid with one of the corresponding Feynman diagrams. The shaded circle is the transversely polarized nucleus, with the vertical double arrow denoting the spin direction.

The Wigner distribution in Eq. (30) allows us to take the quasiclassical GM/MV limit of a large nucleus in a controlled way. For a large "classical" nucleus, we usually can replace $W(p,b)$ with the following classical expression for it (neglecting longitudinal orbital motion of the nucleons):

$$W_{cl}(p,b) = \frac{4\pi}{A}\rho(\underline{b},b^-)\delta\left(p^+ - \frac{P^+}{A}\right)w(\underline{p},b), \tag{31}$$

where $\rho(\underline{b},b^-)$ is the nucleon number density normalized such that

$$\int d^2b db^- \rho(\underline{b},b^-) = A. \tag{32}$$

The function $w(\underline{p},b)$ in Eq. (31) is responsible for the transverse momentum distribution of the nucleons and, to satisfy Eq. (18), is normalized such that

$$\int \frac{d^2p}{(2\pi)^2} w(\underline{p},b) = 1. \tag{33}$$

As originally formulated [26–28], the MV model contained no dependence on the spin or transverse momentum of the valence quarks. This result is recovered by using $w_{\rm MV} = (2\pi)^2\delta^2(\underline{p})$.

Substituting the classical Wigner distribution [Eq. (31)] into Eq. (30) yields

$$\frac{d\sigma^{\gamma^*+A\to q+X}}{d^2{\rm k}dy} = \int \frac{d^2p db^-}{(2\pi)^2} d^2x d^2y \rho\left(\frac{\underline{x}+\underline{y}}{2},b^-\right) w\left(\underline{p},\frac{\underline{x}+\underline{y}}{2},b^-\right) \times \int \frac{d^2k'}{(2\pi)^2} e^{-i(\underline{k}-\underline{k}')\cdot(\underline{x}-\underline{y})} \frac{d\hat{\sigma}^{\gamma^*+N\to q+X}}{d^2k'dy}(p,q) D_{\underline{x}\,\underline{y}}[+\infty,b^-], \tag{34}$$

which is a simplified version of Eq. (30).

B. Quasiclassical Sivers function in SIDIS

Imagine a large nucleus with the total spin $\vec{J}$ such that

$$\vec{J} = \vec{L} + \vec{S}, \tag{35}$$

where $\vec{L}$ is the OAM of all the nucleons in the nucleus and $\vec{S}$ is the net spin of all the nucleons. In the quasiclassical approximation at hand, the OAM is generated by rotation of the nucleons around a preferred axis. The nucleus is transversely polarized to the beam: we assume that both $\vec{L}$ and $\vec{S}$ point along the (positive or negative) $\hat{x}$ axis.

The result [Eq. (30)] for the quark production cross section in SIDIS can be utilized to write down an expression for the SIDIS Sivers function of the large nucleus with the help of Eq. (7b). We first note that the quark production cross section in SIDIS is proportional to the correlator [Eq. (2)] with the future-pointing Wilson line given by Eq. (4) [cf. Eqs. (26) and (27)]. The gauge link in Eq. (27) begins and ends at the same b^-, while the more general gauge link in Eq. (4) has different endpoints at 0 and x^-. The reason is that the nuclear wave function is composed of color-neutral "nucleons" localized in b^-; hence, there is only a contribution to the correlator when the gauge link both begins and ends at the same b^-. The Dirac γ^+ matrix of Eq. (7b) is also present in the quark production cross section, since the Dirac structure of the large-k^- outgoing quark line is given by γ^+k^-. To obtain the Sivers function one only needs to eliminate the gamma matrices stemming from the quark-photon vertices in the amplitude and in the complex conjugate amplitude; this can be done by simply contracting the Lorentz indices of these gamma matrices [21]. While such contraction is not allowed in a calculation of the SIDIS cross section due to nontrivial structure of the lepton tensor, it is a legitimate method of extracting the Sivers function [21], since $\gamma_\mu\gamma^+\gamma^\mu = -2\gamma^+$. We thus see that an equation like Eq. (30) would still hold for ${\rm Tr}[\Phi\gamma^+]$ instead of the SIDIS cross section, since to obtain the former, one simply needs to repeat all the steps of the cross-section derivation that led to Eq. (30) without inserting the photon polarizations [implicit in Eq. (30)] and add a contraction over Lorentz indices of the gamma matrices from the quark-photon vertices in the end.

By analogy with Eq. (30), we can express the quark correlation function Φ_A of the nucleus in terms of the quasiclassical distribution $W_N(p,b)$ of nucleons, the quark correlators ϕ_N of individual nucleons, and the semi-infinite Wilson-line trace $D_{\underline{x}\,\underline{y}}[+\infty,b^-]$:

$$\begin{aligned}{\rm Tr}[\Phi_A(\bar{x},\underline{k};P,J)\gamma^+] = A \int \frac{dp^+d^2pdb^-}{2(2\pi)^3} d^2xd^2y \\ \times \sum_\sigma W_N^\sigma\left(p,b^-,\frac{\underline{x}+\underline{y}}{2}\right) \\ \times \int \frac{d^2k'}{(2\pi)^2} e^{-i(\underline{k}-\underline{k}')\cdot(\underline{x}-\underline{y})} \\ \times {\rm Tr}[\phi_N(x,\underline{k}'-x\underline{p};p,\sigma)\gamma^+] \\ \times D_{\underline{x}\,\underline{y}}[+\infty,b^-].\end{aligned} \tag{36}$$

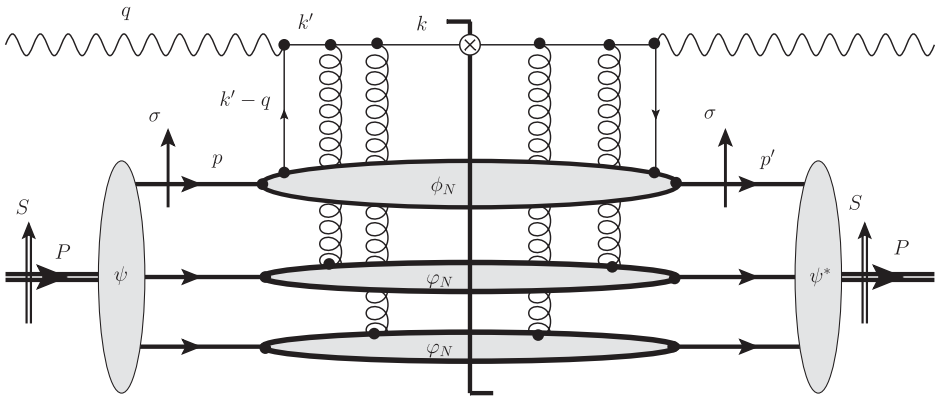

FIG. 5. Decomposition of the nuclear quark distribution Φ_A probed by the SIDIS virtual photon into mean-field wave functions ψ, ψ^* of nucleons and the quark and gluon distributions ϕ_N and ϕ_N of the nucleons.

Equation (36) is illustrated in Fig. 5. In Eq. (36) we explicitly show the sum over the polarizations $\sigma = \pm 1/2$ of the nucleons along the x axis. Note that $x = -q^+/p+$, and it varies with p^+ inside the integral; at the same time, the "averaged" value of Bjorken-x per nucleon is $\bar{x} = -Aq^+/P^+$. The quark correlator of the nucleus Φ_A is defined by Eq. (2),

$$\Phi^A_{ij}(\bar{x}, \underline{k}; P, J) \equiv \int \frac{dx^- d^2x_\perp}{2(2\pi)^3} e^{i(\frac{1}{2}\bar{x}P^+x^- - \underline{x}\cdot\underline{k})} \times \langle A; P, J|\bar{\psi}_j(0)\mathcal{U}^{\rm SIDIS} \times \psi_i(x^+ = 0, x^-, \underline{x})|A; P, J\rangle, \quad (37)$$

along with the corresponding nucleonic correlator:

$$\phi^N_{ij}(x, \underline{k}; p, \sigma) \equiv \int \frac{dx^- d^2x_\perp}{2(2\pi)^3} e^{i(\frac{1}{2}xp^+x^- - \underline{x}\cdot\underline{k})} \times \langle N; p, \sigma|\bar{\psi}_j(0)\mathcal{U}^{\rm SIDIS} \times \psi_i(x^+ = 0, x^-, \underline{x})|N; p, \sigma\rangle. \quad (38)$$

These definitions are done in a frame in which the parent particle's transverse momentum is zero. The $\underline{k}' - x\underline{p}$ in the argument of ϕ_N in Eq. (36) is obtained by making a transverse boost from the frame in which the nucleon has transverse momentum' $\underline{p}$ into a frame in which $\underline{p} = \underline{0}$ [and the definition in Eq. (38) applies]. Note that our lab frame corresponds to the photon-nucleus center-of-mass frame in which $\underline{q} = \underline{P} = \underline{0}$. The polarization-dependent Wigner functions are normalized as [cf. Eq. (18)]

$$\int \frac{dp^+ d^2p db^- d^2b}{2(2\pi)^3} AW^{+1/2}(p, b) = \#\text{spin-up nucleons},$$
$$\int \frac{dp^+ d^2p db^- d^2b}{2(2\pi)^3} AW^{-1/2}(p, b) = \#\text{spin-down nucleons}. \quad (39)$$

As in Ref. [48], the correlation functions in Eq. (36) can be parametrized in terms of the TMD distribution functions, of which the most relevant to the problem at hand are the unpolarized distribution f_1 and the Sivers function $f^\perp_{1T}$. Using Eq. (7), we write

$$\mathrm{Tr}[\Phi_A(\bar{x}, \underline{k}; P, J)\gamma^+] = 2f^A_1(\bar{x}, k_T) + \frac{2}{M_A}\hat{z}\cdot(\underline{J}\times\underline{k})f^{\perp A}_{1T}(\bar{x}, k_T), \quad (40a)$$

$$\mathrm{Tr}[\phi_N(x, \underline{k}' - x\underline{p}; p, \sigma)\gamma^+] = 2f^N_1(x, |\underline{k}' - x\underline{p}|) + \frac{2}{m_N}\hat{z}\cdot(\underline{\sigma}\times(\underline{k}' - x\underline{p}))f^{\perp N}_{1T}(x, |\underline{k}' - x\underline{p}|), \quad (40b)$$

where we introduce the unpolarized quark TMDs (f^A_1 and f^N_1) and Sivers functions ($f^{\perp A}_{1T}$ and $f^{\perp N}_{1T}$) for the nucleus and nucleons, respectively, along with the masses M_A and m_N of the nucleus and nucleons.

We may extract the Sivers function of the nucleus $f^{\perp A}_{1T}$ by antisymmetrizing Eq. (40a) with respect to either the nuclear spin or the momentum $\underline{k}$ of the produced quark[5]:

$$\hat{z}\cdot(\underline{J}\times\underline{k})f^{\perp A}_{1T}(\bar{x}, k_T) = \frac{1}{4}M_A\mathrm{Tr}[\Phi_A(\bar{x}, \underline{k}; P, J)\gamma^+] - (\underline{k} \to -\underline{k}). \quad (41)$$

Using Eq. (36) in Eq. (41), we write

[5]In doing so, we assume that the Sivers function is an even function of $\underline{k}$, which is indeed the case due to its T-symmetry properties.

$$\hat{z}\cdot(\underline{J}\times\underline{k})f_{1T}^{\perp A}(\bar{x},k_T)=\frac{1}{4}M_A A\int\frac{dp^+d^2pdb^-}{2(2\pi)^3}d^2xd^2y\sum_\sigma W_N^\sigma\left(p,b^-,\frac{\underline{x}+\underline{y}}{2}\right)$$
$$\times\int\frac{d^2k'}{(2\pi)^2}e^{-i(\underline{k}-\underline{k}')\cdot(\underline{x}-\underline{y})}\mathrm{Tr}[\phi_N(x,\underline{k}'-x\underline{p};p,\sigma)\gamma^+]D_{\underline{x}\,\underline{y}}[+\infty,b^-]-(\underline{k}\to-\underline{k}). \quad (42)$$

We can decompose the quark correlator in a nucleon ϕ_N into the nucleon's unpolarized quark distribution f_1^N and Sivers function f_{1T}^N using Eq. (40b). Substituting this into Eq. (42) yields

$$\hat{z}\cdot(\underline{J}\times\underline{k})f_{1T}^{\perp A}(\bar{x},k_T)=\frac{1}{4}M_A A\int\frac{dp^+d^2pdb^-}{2(2\pi)^3}d^2xd^2y\sum_\sigma W_N^\sigma\left(p,b^-,\frac{\underline{x}+\underline{y}}{2}\right)\int\frac{d^2k'}{(2\pi)^2}e^{-i(\underline{k}-\underline{k}')\cdot(\underline{x}-\underline{y})}$$
$$\times\left[2f_1^N(x,|\underline{k}'-x\underline{p}|)+\frac{2}{m_N}\hat{z}\cdot(\underline{\sigma}\times(\underline{k}'-x\underline{p}))\,f_{1T}^{\perp N}(x,|\underline{k}'-x\underline{p}|)\right]D_{\underline{x}\,\underline{y}}[+\infty,b^-]-(\underline{k}\to-\underline{k}). \quad (43)$$

We can understand the sources of the T-odd nuclear Sivers function $f_{1T}^{\perp A}$ by explicitly (anti)symmetrizing the various terms on the right of Eq. (43). To start with, we perform the nucleon spin sum $\sum_\sigma$ in a basis parallel or antiparallel to the nuclear spin $\underline{S}$. This can be done using the definitions

$$\sum_\sigma W_N^\sigma(p,b)\equiv W_{\mathrm{unp}}(p,b),$$
$$\sum_\sigma W_N^\sigma(p,b)\underline{\sigma}\equiv\frac{1}{A}W_{\mathrm{trans}}(p,b)\underline{S}, \quad (44)$$

where we will refer to W_{unp} as the distribution of unpolarized nucleons and to W_{trans} as the nucleon transversity distribution. Note that

$$\int\frac{dp^+d^2pdb^-d^2b}{2(2\pi)^3}W_{\mathrm{unp}}(p,b)=1,$$
$$\int\frac{dp^+d^2pdb^-d^2b}{2(2\pi)^3}W_{\mathrm{trans}}(p,b)=1, \quad (45)$$

as follows from the definition in Eq. (44) and from Eq. (39).

Equation (43) becomes

$$\hat{z}\cdot(\underline{J}\times\underline{k})f_{1T}^{\perp A}(\bar{x},k_T)=\frac{M_A}{2}\int\frac{dp^+d^2pdb^-}{2(2\pi)^3}d^2xd^2y\frac{d^2k'}{(2\pi)^2}e^{-i(\underline{k}-\underline{k}')\cdot(\underline{x}-\underline{y})}$$
$$\times\left[AW_{\mathrm{unp}}\left(p,b^-,\frac{\underline{x}+\underline{y}}{2}\right)f_1^N(x,|\underline{k}'-x\underline{p}|)+W_{\mathrm{trans}}\left(p,b^-,\frac{\underline{x}+\underline{y}}{2}\right)\frac{1}{m_N}\hat{z}\right.$$
$$\left.\cdot(\underline{S}\times(\underline{k}'-x\underline{p}))f_{1T}^{\perp N}(x,|\underline{k}'-x\underline{p}|)\right]D_{\underline{x}\,\underline{y}}[+\infty,b^-]-(\underline{k}\to-\underline{k}). \quad (46)$$

Now, in the terms with $(\underline{k}\to-\underline{k})$ being subtracted, we also redefine the dummy integration variables $\underline{x}\leftrightarrow\underline{y}$, $\underline{k}'\to-\underline{k}'$, and $\underline{p}\to-\underline{p}$. This leaves the Fourier factors and the distribution functions f_1^N, $f_{1T}^{\perp N}$ unchanged, giving

$$\hat{z}\cdot(\underline{J}\times\underline{k})f_{1T}^{\perp A}(\bar{x},k_T)=\frac{M_A}{2}\int\frac{dp^+d^2pdb^-}{2(2\pi)^3}d^2xd^2y\frac{d^2k'}{(2\pi)^2}e^{-i(\underline{k}-\underline{k}')\cdot(\underline{x}-\underline{y})}\left\{f_1^N(x,|\underline{k}'-x\underline{p}|)\right.$$
$$\times A\left[W_{\mathrm{unp}}\left(p^+,\underline{p},b^-,\frac{\underline{x}+\underline{y}}{2}\right)D_{\underline{x}\,\underline{y}}[+\infty,b^-]-W_{\mathrm{unp}}\left(p^+,-\underline{p},b^-,\frac{\underline{x}+\underline{y}}{2}\right)D_{\underline{y}\,\underline{x}}[+\infty,b^-]\right]$$
$$+\frac{1}{m_N}\hat{z}\cdot(\underline{S}\times(\underline{k}'-x\underline{p}))f_{1T}^{\perp N}(x,|\underline{k}'-x\underline{p}|)$$
$$\left.\times\left[W_{\mathrm{trans}}\left(p^+,\underline{p},b^-,\frac{\underline{x}+\underline{y}}{2}\right)D_{\underline{x}\,\underline{y}}[+\infty,b^-]+W_{\mathrm{trans}}\left(p^+,-\underline{p},b^-,\frac{\underline{x}+\underline{y}}{2}\right)D_{\underline{y}\,\underline{x}}[+\infty,b^-]\right]\right\}. \quad (47)$$

At this point, it is convenient to explicitly (anti)symmetrize the distribution functions with respect to $\underline{p}\leftrightarrow-\underline{p}$ and the Wilson lines with respect to $\underline{x}\leftrightarrow\underline{y}$. We define

$$S_{\underline{x}\,\underline{y}} \equiv \tfrac{1}{2}(D_{\underline{x}\,\underline{y}} + D_{\underline{y}\,\underline{x}}),$$
$$iO_{\underline{x}\,\underline{y}} \equiv \tfrac{1}{2}\left(D_{\underline{x}\,\underline{y}} - D_{\underline{y}\,\underline{x}}\right), \qquad D_{\underline{x}\,\underline{y}} = S_{\underline{x}\,\underline{y}} + iO_{\underline{x}\,\underline{y}} \tag{48}$$

and

$$W^{(\mathrm{symm}\atop \mathrm{OAM})}(p,b) \equiv \frac{1}{2}[W(p,b) \pm (\underline{p} \to -\underline{p})], \tag{49}$$

where we have used the "OAM" label to indicate that the preferred direction of transverse momentum in the antisymmetric case reflects the presence of net orbital angular momentum. We can decompose W into symmetric and OAM parts for both the unpolarized distribution W_{unp} and the transversity distribution W_{trans}.

Using the (anti)symmetrized quantities in Eq. (49), we can evaluate the factors in the square brackets of Eq. (47) as

$$\begin{aligned} W_{\mathrm{unp}}(p,b)D_{\underline{x}\,\underline{y}}[+\infty,b^-] - W_{\mathrm{unp}}(-\underline{p},b)D_{\underline{y}\,\underline{x}}[+\infty,b^-] &= 2(W^{\mathrm{OAM}}_{\mathrm{unp}}(p,b)S_{\underline{x}\,\underline{y}}[+\infty,b^-] + W^{\mathrm{symm}}_{\mathrm{unp}}(p,b)iO_{\underline{x}\,\underline{y}}[+\infty,b^-]), \\ W_{\mathrm{trans}}(p,b)D_{\underline{x}\,\underline{y}}[+\infty,b^-] + W_{\mathrm{trans}}(-\underline{p},b)D_{\underline{y}\,\underline{x}}[+\infty,b^-] &= 2(W^{\mathrm{symm}}_{\mathrm{trans}}(p,b)S_{\underline{x}\,\underline{y}}[+\infty,b^-] + W^{\mathrm{OAM}}_{\mathrm{trans}}(p,b)iO_{\underline{x}\,\underline{y}}[+\infty,b^-]), \end{aligned} \tag{50}$$

giving

$$\begin{aligned} \hat{z}\cdot(\underline{J}\times\underline{k})f_{1T}^{\perp A}(\bar{x},k_T) = M_A \int \frac{dp^+d^2pdb^-}{2(2\pi)^3}d^2xd^2y\frac{d^2k'}{(2\pi)^2}e^{-i(\underline{k}-\underline{k}')\cdot(\underline{x}-\underline{y})}\Bigg\{ & f_1^N(x,|\underline{k}'-x\underline{p}|) \\ & \times A\left[W^{\mathrm{OAM}}_{\mathrm{unp}}\left(p^+,\underline{p},b^-,\frac{\underline{x}+\underline{y}}{2}\right)S_{\underline{x}\,\underline{y}}[+\infty,b^-] + W^{\mathrm{symm}}_{\mathrm{unp}}\left(p^+,\underline{p},b^-,\frac{\underline{x}+\underline{y}}{2}\right)iO_{\underline{x}\,\underline{y}}[+\infty,b^-]\right] \\ & + \frac{1}{m_N}\hat{z}\cdot(\underline{S}\times(\underline{k}'-x\underline{p}))f_{1T}^{\perp N}(x,|\underline{k}'-x\underline{p}|) \\ & \times\left[W^{\mathrm{symm}}_{\mathrm{trans}}\left(p^+,\underline{p},b^-,\frac{\underline{x}+\underline{y}}{2}\right)S_{\underline{x}\,\underline{y}}[+\infty,b^-] + W^{\mathrm{OAM}}_{\mathrm{trans}}\left(p^+,\underline{p},b^-,\frac{\underline{x}+\underline{y}}{2}\right)iO_{\underline{x}\,\underline{y}}[+\infty,b^-]\right]\Bigg\}. \end{aligned} \tag{51}$$

Altogether, the symmetry arguments presented above allow us to decompose the nuclear Sivers function $f_{1T}^{\perp A}$ into four distinct channels with the right quantum numbers to generate the T-odd asymmetry. These four channels correspond to the negative T parity occurring in the nucleon distribution W^{OAM}, in the quark Sivers function of the nucleon $f_{1T}^{\perp N}$, in the antisymmetric "odderon" rescattering iO_{xy}, or in all three simultaneously.

We will now neglect the odderon contributions in Eq. (51). The way to understand this approximation is as follows: As shown in Ref. [17], the preferred direction generated by odderon-type rescattering couples to transverse gradients of the nuclear profile function, $\underline{\nabla}T(\underline{b})$. The length scale over which these gradients become important is on the order of the nuclear radius; these gradients are therefore $\mathcal{O}(A^{-1/3}) \sim \mathcal{O}(\alpha_s^2)$ suppressed (in addition to an extra power of α_s entering the lowest-order odderon amplitude corresponding to the triple-gluon exchange [17,52–59]) and are beyond the precision of the quasiclassical formula [Eq. (51)].

Neglecting the odderon channels in Eq. (51), we arrive at

$$\begin{aligned} \hat{z}\cdot(\underline{J}\times\underline{k})f_{1T}^{\perp A}(\bar{x},k_T) = M_A \int \frac{dp^+d^2pdb^-}{2(2\pi)^3}d^2xd^2y\frac{d^2k'}{(2\pi)^2}e^{-i(\underline{k}-\underline{k}')\cdot(\underline{x}-\underline{y})} & \\ \times\Bigg\{AW^{\mathrm{OAM}}_{\mathrm{unp}}\left(p^+,\underline{p},b^-,\frac{\underline{x}+\underline{y}}{2}\right)f_1^N(x,|\underline{k}'-x\underline{p}|) & \\ + \frac{1}{m_N}\hat{z}\cdot(\underline{S}\times(\underline{k}'-x\underline{p}))W^{\mathrm{symm}}_{\mathrm{trans}}\left(p^+,\underline{p},b^-,\frac{\underline{x}+\underline{y}}{2}\right)f_{1T}^{\perp N}(x,|\underline{k}'-x\underline{p}|)\Bigg\}S_{\underline{x}\,\underline{y}}[+\infty,b^-]. & \end{aligned} \tag{52}$$

Shifting the integration variable $\underline{k}' \to \underline{k}' + x\underline{p}$, we write

$$\hat{z}\cdot(\underline{J}\times\underline{k})f_{1T}^{\perp A}(\bar{x},k_T) = M_A\int\frac{dp^+d^2p db^-}{2(2\pi)^3}d^2xd^2y\frac{d^2k'}{(2\pi)^2}e^{-i(\underline{k}-x\underline{p}-\underline{k}')\cdot(\underline{x}-\underline{y})}\left\{AW_{\rm unp}^{\rm OAM}\left(p^+,\underline{p},b^-,\frac{\underline{x}+\underline{y}}{2}\right)f_1^N(x,k_T') + \frac{1}{m_N}\hat{z}\cdot(\underline{S}\times\underline{k}')W_{\rm trans}^{\rm symm}\left(p^+,\underline{p},b^-,\frac{\underline{x}+\underline{y}}{2}\right)f_{1T}^{\perp N}(x,k_T')\right\}S_{\underline{x}\,\underline{y}}[+\infty,b^-]. \tag{53}$$

To further simplify the obtained expression [Eq. (53)], we need to impose a constraint on the transverse momentum of the nucleons. Consider the nucleus in its rest frame, as shown in Fig. 6. The net OAM $\vec{L}$ of the transversely polarized nucleus corresponds to the rotation of the nucleus around the spin axis (the x axis in Fig. 6). The rotational invariance around the x axis implies that the average magnitude of the rotational transverse momentum is constant for a given distance from the x axis and for a fixed x coordinate. (In Appendix B, we show that, as a consequence of PT symmetry, only rotational motion of the nucleons in the nucleus rest frame is allowed.)

Consider a nucleon at the point $\vec{x} = (0,-R,0)$ in the (x,y,z) coordinate system, as illustrated by the black circle in Fig. 6. Its three-momentum is $\vec{p}_{\rm rest} = (0,0,-p)$, where p denotes some typical rotational momentum of a nucleon. After a longitudinal boost along the z axis to the infinite-momentum frame of Eq. (8), we find the large light-cone component of the momentum to be

$$p^+ = \frac{P^+}{M_A}\left(\sqrt{m_N^2+p^2}-p\right). \tag{54}$$

The corresponding Bjorken-x is [see Eq. (9)]

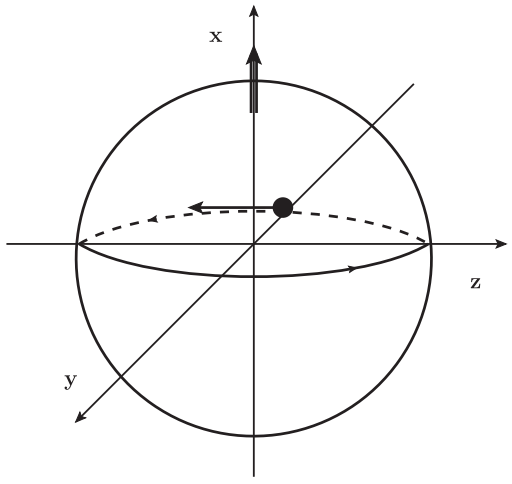

FIG. 6. This figure demonstrates our axis-labeling convention and helps illustrate an example discussed in the text.

$$1 \geq x = \frac{-q^+}{p^+} = x_A A\frac{m_N}{\sqrt{m_N^2+p^2}-p}, \tag{55}$$

where we have used $M_A = Am_N$. The $x \leq 1$ constraint in Eq. (55) [cf. Eq. (9)] gives

$$p \leq m_N\frac{1-x_A^2A^2}{2x_AA}. \tag{56}$$

Since x_AA is not a small number—in fact, $x_AA = \mathcal{O}(1)$—we conclude that $p \lesssim m_N$. Therefore, the magnitude of the rotational momentum in the nuclear rest frame is bounded by $\sim m_N$ from above. The typical transverse momentum p_T in Eq. (53), being boost invariant, is also bounded by the nucleon mass from above, $p_T \lesssim m_N$. Since we assume that k_T is perturbatively large, $k_T \gg \Lambda_{\rm QCD} \sim m_N$, we do not consistently resum all powers of m_N/k_T. (The saturation approach resums mainly $A^{1/3}$-enhanced power corrections —that is, powers of Q_s^2/k_T^2, but not powers of $\Lambda_{\rm QCD}^2/k_T^2$.)

The bound in Eq. (56) provides us with the condition on when the SIDIS process on the nucleon highlighted in Fig. 6 can take place. Violation of this bound would imply that SIDIS on that nucleon is kinematically prohibited, and consequently SIDIS may take place only on some of the other nucleons in the nucleus. While such a situation where the nucleus is spinning so fast that SIDIS is only possible on a subset of its nucleons is highly unlikely in the real physical experiments, this presents a theoretical example where the Sivers function [Eq. (53)] would, in fact, depend on the direction of $\underline{p}$ and, hence, of spin $\underline{J}$, presumably through even powers of $\underline{J}\cdot\underline{k}$. While such dependence is impossible for spin-1/2 particles such as protons [60], it has been considered for targets with different spin [61]; in our case, it arises due to the classical model at hand with the value of spin J not restricted to 1/2. To avoid potential formal complications and unrealistic effects associated with large rotational momentum, below we will assume that $p_T \lesssim m_N$ such that the bound in Eq. (56) is satisfied. Without such assumption, Eq. (53) would be our final result for the Sivers function in the quasiclassical approximation.

We see that we have to limit the calculation to the lowest nontrivial power of $p_T/k_T \sim m_N/k_T$ contributing to the Sivers function. Expanding Eq. (53) in the powers of $\underline{p}$ to the lowest nontrivial order, and remembering that $W^{\rm OAM}$ is an odd function of $\underline{p}$, we obtain

$$\hat{z}\cdot(\underline{J}\times\underline{k})f_{1T}^{\perp A}(\bar{x},k_T)=M_A\int\frac{dp^+d^2pdb^-}{2(2\pi)^3}d^2xd^2y\frac{d^2k'}{(2\pi)^2}e^{-i(\underline{k}-\underline{k}')\cdot(\underline{x}-\underline{y})}$$
$$\times\left\{ix\underline{p}\cdot(\underline{x}-\underline{y})AW_{\rm unp}^{\rm OAM}\left(p^+,\underline{p},b^-,\frac{\underline{x}+\underline{y}}{2}\right)f_1^N(x,k_T')\right.$$
$$\left.+\frac{1}{m_N}\hat{z}\cdot\left(\underline{S}\times\underline{k}'\right)W_{\rm trans}^{\rm symm}\left(p^+,\underline{p},b^-,\frac{\underline{x}+\underline{y}}{2}\right)f_{1T}^{\perp N}(x,k_T')\right\}S_{\underline{x}\,\underline{y}}[+\infty,b^-]. \quad (57)$$

Equation (57) is our main formal result. It relates the Sivers function of a nucleus to the quark TMD and quark Sivers function in a nucleon. It shows that within the quasiclassical approximation, there are two leading channels capable of generating the Sivers function of the composite nucleus:

(1) *Orbital angular momentum (OAM) channel:* An unpolarized nucleon in a transversely polarized nucleus with a preferred direction of transverse momentum generated by the OAM of the nucleus has a quark knocked out of its symmetric f_1^N transverse momentum distribution which rescatters coherently on spectator nucleons. The multiple rescatterings bias the initial knockout process to happen near the "back" of the nucleus, where, due to OAM motion of the nucleons, the outgoing quark gets an asymmetric distribution of its transverse momentum, generating STSA. (See Fig. 2 or left panel of Fig. 7 below.)

(2) *Transversity/Sivers density channel:* A polarized nucleon with its preferred transverse spin direction inherited from the nucleus has a quark knocked out of its Sivers $f_{1T}^{\perp N}$ distribution which rescatters coherently on spectator nucleons. The single spin asymmetry is generated at the level of the "first" nucleon, and unlike the OAM channel, the presence of other nucleons is not essential for this channel (see Fig. 7).

The OAM and transversity channels are depicted in Fig. 7 in terms of their space-time structure and Feynman diagrams. The diagrams resummed in arriving at Eq. (57) are the square of the graph shown in the left panel of Fig. 7 (OAM channel) and the diagram looking like the interference between the two panels in Fig. 7 (transversity channel). The difference between the two channels outlined above is in the first "knockout" interaction: the OAM channel couples to quark TMD, while the transversity channel couples to the nucleon Sivers function. At the lowest order in perturbation theory the two functions are illustrated in Fig. 8: indeed, the Sivers function shown in panel B of Fig. 8 requires at least one more rescattering as compared to the quark TMD in panel A, according to the conventional wisdom [10,11].

Note that, in the OAM channel, the unpolarized quark distribution f_1^N enters parametrically at $\mathcal{O}(\alpha_s A^{1/3})$ if calculated at the lowest order in the perturbation theory (see panel A in Fig. 8), which is $\mathcal{O}(\alpha_s^{-1})$ in the saturation power counting (where $\alpha_s^2 A^{1/3}\sim 1$). In the transversity channel, the nucleonic Sivers function $f_{1T}^{\perp N}$ enters at $\mathcal{O}(\alpha_s^2 A^{1/3})=\mathcal{O}(1)$ at the lowest order in

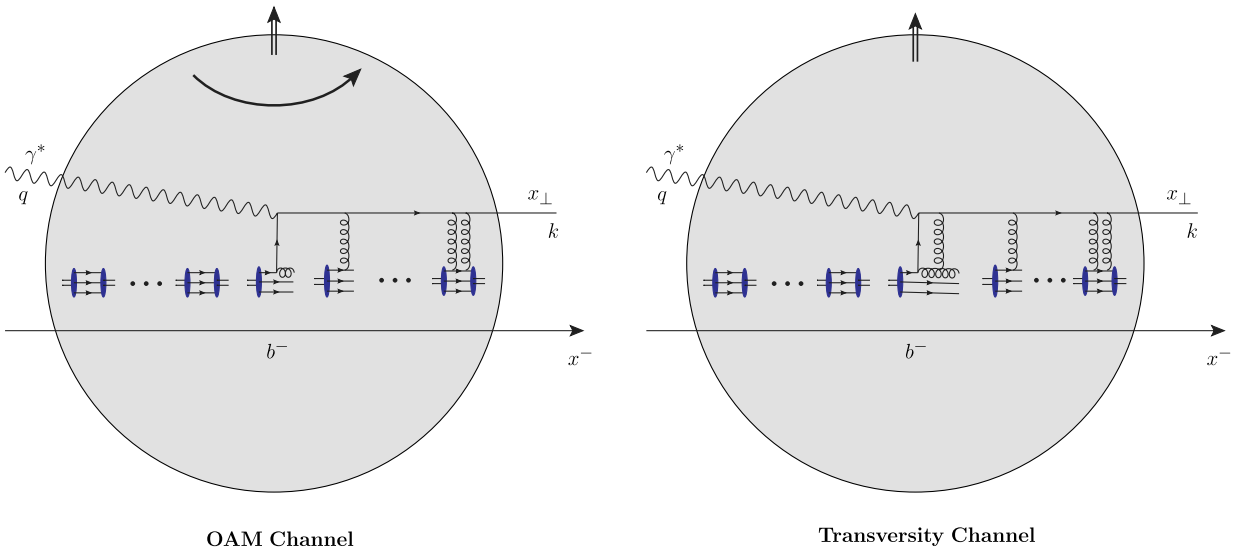

FIG. 7 (color online). Side-by-side comparison of the Feynman diagram's contribution to the OAM and Sivers density channels in the quasiclassical approximation (in the rest frame of the nucleus).

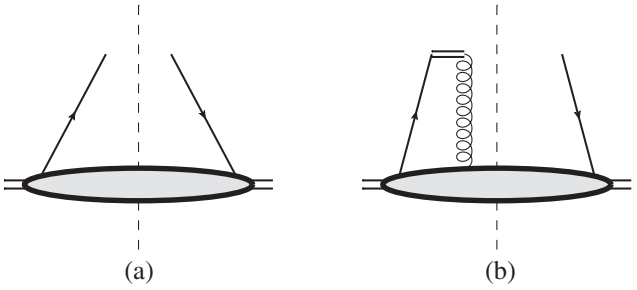

FIG. 8. Lowest-order diagrams for the quark TMD f_1 (panel A) and the Sivers function $f_{1T}^{\perp}$ (panel B). The vertical dashed line denotes the final-state cut, while the double horizontal line in panel B denotes the Wilson line.

perturbation theory, because it requires an extra $\mathcal{O}(\alpha_s)$ gluon to be exchanged with the same nucleon to obtain the necessary lensing effect [10] (see panel B in Fig. 8). The transversity channel is therefore $\mathcal{O}(1)$ in the saturation power counting and is subleading by $\mathcal{O}(\alpha_s)$ to the OAM channel in this sense.[6] Indeed, the nontrivial transverse motion of nucleons due to OAM should be present in order for the OAM channel to be nonzero: this channel is leading only if there is an OAM. In our estimate here, we have assumed that the net spin of our "nucleons" scales linearly with the atomic number, $S \sim A$; perhaps a more realistic (both for protons and nuclei) slower growth of S with A would introduce extra A suppression for the transversity channel.

Despite the transversity channel being subleading, it is more dominant than the $\mathcal{O}(A^{-1/3}) \sim \mathcal{O}(\alpha_s^2)$ corrections we neglected when arriving at the quasiclassical formula [Eq. (57)] (again, for $S \sim A$). Order-α_s^1 quantum corrections to the OAM channel also enter at the same order as the nucleonic Sivers function and are also within the precision of the formalism.

An essential role is played by the rescattering factor $S_{\underline{x}\,y}[+\infty, b^-]$ in the OAM channel. The Wigner function due to the orbital motion of nucleons around the axis of the transverse spin is an odd function of the longitudinal coordinate b_z in the rest frame of the nucleus,

$$W_{\rm unp}^{\rm OAM}(p, \underline{b}, b_z) = -W_{\rm unp}^{\rm OAM}(p, \underline{b}, -b_z), \tag{58}$$

which follows simply from the fact that in the left panel of Fig. 7 we have as many nucleons moving outside the page to the left of the nuclear center as there are nucleons moving into the page to the right of the nuclear center. In Appendix B, we show how the result [Eq. (58)] can be obtained by requiring that our "nucleus" be PT symmetric. The b^- integral of the first term in the curly brackets of Eq. (57) would have been zero, if it were not for the b^--dependent factor of $S_{\underline{x}\,y}[+\infty, b^-]$. This multiple rescattering factor approaches $\bar{1}$ for b^- values near the "back" of the nucleus (the right end of the nucleus in Fig. 7) and is a monotonically decreasing function of b^-. Due to this factor, different b^- regions contribute differently to the integral, making it nonzero. The region near the "back" of the nucleus dominates, which has a physical interpretation that it is easier for the quark to escape the nucleus if it is produced near the edge. Hence, we arrive at the interpretation of the SIDIS in the OAM channel outlined in the Introduction: the quarks are produced predominantly toward the "back" of the nucleus, where the nucleons rotate preferentially into the page (see the left panels of Figs. 7 or 2). Therefore, the quark has more transverse momentum into the page than out of the page, which leads to STSA for the produced quarks.

To complete Eq. (57), we need to construct an expression for the nuclear spin $\vec{J} = \vec{L} + \vec{S}$. The OAM of the nucleons in the nucleus from Fig. 6 in the nuclear rest frame is

$$\begin{aligned}\vec{L} &= A \int \frac{d^3p\, d^3b}{2(2\pi)^3} W_{\rm unp}(\vec{p}, \vec{b}) \vec{b} \times \vec{p} \\ &= A \int \frac{d^3p\, d^3b}{2(2\pi)^3} W_{\rm unp}(\vec{p}, \vec{b}) \hat{x} (b_y p_z - b_z p_y),\end{aligned} \tag{59}$$

where $d^3p = dp_x dp_y dp_z$, $d^3b = db_x db_y db_z$, and $W_{\rm unp}(\vec{p}, \vec{b})$ is the Wigner distribution in the rest frame of the nucleus expressed in terms of three-vectors $\vec{p} = (p_x, p_y, p_z)$ and $\vec{b} = (b_x, b_y, b_z)$.

To boost this into the infinite-momentum frame of Eq. (8), we define the Pauli-Lubanski vector of the nuclear spin,

$$W_\mu = -\frac{1}{2} \epsilon_{\mu\nu\rho\sigma} J^{\nu\rho} P^\sigma, \tag{60}$$

where $J_{\mu\nu} = L_{\mu\nu} + S_{\mu\nu}$, with $L_{\mu\nu}$ and $S_{\mu\nu}$ the expectation values of the OAM and spin generators of the Lorentz group in the nuclear state. The OAM generator is

$$\hat{L}_{\mu\nu} = \hat{x}_\mu \hat{p}_\nu - \hat{x}_\nu \hat{p}_\mu \tag{61}$$

as usual, with the hat denoting operators. The nuclear OAM four-vector is then defined by

$$L_\mu = -\frac{1}{2} \epsilon_{\mu\nu\rho\sigma} L^{\nu\rho} \frac{P^\sigma}{M_A}. \tag{62}$$

Note that $\hat{p}_\mu$ in Eq. (61) are the momentum operators of the nucleons, while P^σ in Eqs. (60) and (62) is the net momentum

[6] We would like to point out that the coupling constant α_s in f_1^N runs with some nonperturbative momentum scale, and is large, $\alpha_s = \alpha_s(\sim \Lambda_{\rm QCD}^2)$; however, a simple application of the BLM [51] prescription to the calculation of Ref. [21] can show that in $f_{1T}^{\perp N}(x, k_T)$ the two powers of the coupling run as $\alpha_s(k_T^2)\alpha_s(\sim \Lambda_{\rm QCD}^2)$. While one of the couplings is also nonperturbatively large, the other one is perturbatively small for $k_T \gg \Lambda_{\rm QCD}$, indicating suppression.

of the whole nucleus. In the rest frame of the nucleus, Eq. (62) gives $L_x = L_{yz}$ as expected (for $\epsilon_{0123} = +1$). The nuclear OAM four-vector can then be written as

$$L_\mu = -\frac{1}{2}\epsilon_{\mu\nu\rho\sigma}\frac{P^\sigma}{M_A}A\int\frac{dp^+d^2pdb^-d^2b}{2(2\pi)^3} \times W_{\rm unp}(p,b)(b^\nu p^\rho - b^\rho p^\nu) \tag{63}$$

in the infinite-momentum frame of the nucleus.

Since boosts preserve transverse components of four-vectors, the boost along the $\hat{z}$ axis of the nucleus in Fig. 6 would preserve its OAM three-vector $\vec{L}$. Hence, Eq. (59) gives us the transverse components of OAM in the infinite-momentum frame as well. We thus write

$$\vec{J} = \hat{x}\left[S + A\int\frac{d^3pd^3b}{2(2\pi)^3}W_{\rm unp}(\vec{p},\vec{b})\hat{x}(b_yp_z - b_zp_y)\right], \tag{64}$$

where the integration over p and b needs to be carried out in the nucleus rest frame.

Combining Eqs. (57) with (64) allows one to extract the Sivers function $f_{1T}^{\perp A}$ of the nucleus.

C. Comparison of the OAM and transversity channels in the SIDIS Sivers function

We will now illustrate the properties of the Sivers function [Eq. (57)] by studying a specific simplified example. Consider the model of the nucleus as a nonrelativistic rigid rotator, with the rotational momentum in its rest frame being much smaller than the nucleon mass, $p_T \ll m_N$. The corresponding classical Wigner distribution is [cf. Eq. (31)]

$$W_{\rm unp}(p,b) \approx \frac{2(2\pi)^3}{A}\rho(\underline{b},b^-)\delta^2\left(\underline{p} - \hat{y}p_{\rm max}(b_x)\frac{b^-}{R^-(b_x)}\right) \times \delta\left(p^+ - \frac{P^+}{A}\right), \tag{65}$$

where $2R^-(b_x)$ is the extent of the nucleus in the b^- direction at $\underline{b} = (b_x, 0)$ [with $R^-(b_x) = \sqrt{R^2 - b_x^2}M_A/P^+$], and $p_{\rm max}(b_x) = p_{\rm max}\sqrt{R^2 - b_x^2}/R$ is the maximum value of the rotational momentum at a given b_x. In writing down the distribution in Eq. (65), we have neglected possible longitudinal rotational motion of the nucleons, which is justified in the $p_T \ll m_N$ limit. We also assume that a fraction β of the nucleons in the nucleus are polarized in the $+\hat{x}$ direction, such that their net spin is $S = \beta A/2$ and [see Eq. (44)]

$$W_{\rm trans}(p,b) = \beta W_{\rm unp}(p,b). \tag{66}$$

Substituting Eqs. (65) and (66) into Eq. (57) and integrating over p^+ and $\underline{p}$ yields

$$Jk_yf_{1T}^{\perp A}(\bar{x},k_T) = M_A\int db^-d^2xd^2y\rho\left(\frac{\underline{x}+\underline{y}}{2},b^-\right)\frac{d^2k'}{(2\pi)^2}e^{-i(\underline{k}-\underline{k}')\cdot(\underline{x}-\underline{y})}\left\{i\bar{x}p_{\rm max}\left(\frac{(\underline{x}+\underline{y})_x}{2}\right)\frac{b^-}{R^-\left(\left(\frac{x+y}{2}\right)_x\right)}(\underline{x}-\underline{y})_yf_1^N(\bar{x},k'_T) + \frac{\beta}{2m_N}k'_yf_{1T}^{\perp N}(\bar{x},k'_T)\right\}S_{\underline{x}\,\underline{y}}[+\infty,b^-], \tag{67}$$

where we also replace $\vec{J}$ with $\hat{x}J$ and $\vec{S}$ with $\hat{x}(\beta A/2)$.

To further simplify Eq. (67), we need to make specific assumptions about the form of f_1^N and $f_{1T}^{\perp N}$. Inspired by the lowest-order expressions for both quantities [21,48,62], we write

$$f_1^N(x,k_T) = \frac{\alpha_sC_1}{k_T^2}, \qquad f_{1T}^{\perp N}(x,k_T) = \frac{\alpha_s^2m_N^2C_2}{k_T^4}\ln\frac{k_T^2}{\Lambda^2}, \tag{68}$$

where C_1 and C_2 are some x-dependent functions and Λ is an infrared cutoff. Inserting Eq. (68) into Eq. (67) and integrating over k'_T yields

$$Jk_yf_{1T}^{\perp A}(\bar{x},k_T) = \frac{\alpha_sM_A}{2\pi}\int db^-d^2xd^2y\rho\left(\frac{\underline{x}+\underline{y}}{2},b^-\right)e^{-i\underline{k}\cdot(\underline{x}-\underline{y})}(\underline{x}-\underline{y})_y\left\{i\bar{x}p_{\rm max}\left(\frac{(\underline{x}+\underline{y})_x}{2}\right)\frac{b^-C_1}{R^-\left(\left(\frac{x+y}{2}\right)_x\right)} \times \ln\frac{1}{|\underline{x}-\underline{y}|\Lambda} + \frac{i\alpha_sm_N\beta C_2}{4}\ln^2\frac{1}{|\underline{x}-\underline{y}|\Lambda}\right\}S_{\underline{x}\,\underline{y}}[+\infty,b^-]. \tag{69}$$

In the classical MV/GM approximation, the (symmetric part of the) dipole scattering matrix is [25]

$$S_{\underline{x}\,\underline{y}}[+\infty, b^-] = \exp\left[-\frac{1}{4}|\underline{x}-\underline{y}|^2 Q_s^2\left(\frac{\underline{x}+\underline{y}}{2}\right) \times \left(\frac{R^-(\underline{b})-b^-}{2R^-(\underline{b})}\right) \ln\frac{1}{|\underline{x}-\underline{y}|\Lambda}\right], \quad (70)$$

where $R^-(\underline{b}) = \sqrt{R^2-\underline{b}^2}M_A/P^+$, and the quark saturation scale is

$$Q_s^2(\underline{b}) = 4\pi\alpha_s^2\frac{C_F}{N_c}T(\underline{b}) \quad (71)$$

with the nuclear profile function

$$T(\underline{b}) = \int db^- \rho(\underline{b}, b^-). \quad (72)$$

As usual, N_c is the number of colors, and $C_F = (N_c^2-1)/2N_c$ is the Casimir operator of SU(N_c) in the fundamental representation. In arriving at Eq. (70), we assume that the nuclear density is constant within the nucleus, such that

$$\rho(\underline{b}, b^-) = \frac{\theta\left(R^-(\underline{b})-|b^-|\right)}{2R^-(\underline{b})}T(\underline{b}). \quad (73)$$

Employing Eq. (70) along with Eqs. (73) and (71), and neglecting all logarithms $\ln(1/|\underline{x}-\underline{y}|\Lambda)$ (which is justified as long as k_T is not too much larger than Q_s [63]), we can integrate Eq. (69) over b^- and $\underline{x}-\underline{y}$, obtaining

$$f_{1T}^{\perp A}(\bar{x}, k_T) = \frac{M_A N_c}{4\pi\alpha_s J C_F}\frac{1}{k_T^2}\int d^2b\left\{4\bar{x}p_{\max}(\underline{b})C_1 \times\left[e^{-k_T^2/Q_s^2(\underline{b})} + 2\frac{k_T^2}{Q_s^2(\underline{b})}Ei\left(-\frac{k_T^2}{Q_s^2(\underline{b})}\right)\right] + \alpha_s\beta m_N C_2 e^{-k_T^2/Q_s^2(\underline{b})}\right\}, \quad (74)$$

where now $\underline{b} = (\underline{x}+\underline{y})/2$ and $p_{\max}(\underline{b}) = p_{\max}\sqrt{R^2-\underline{b}^2}/R$. The $\underline{b}$ integral appears to be rather hard to perform for a realistic spherical nucleus: we leave expression (74) in its present form.

To obtain a final expression for the Sivers function, we need to determine the spin of the nucleus J. For a rigid rotator spinning around the $\hat{x}$ axis with the maximum nucleon momentum $p_{\max}$, we readily get

$$L = \frac{4}{5}Ap_{\max}R \quad (75)$$

in the nuclear rest frame. Using this in Eq. (64) along with $S = \beta A/2$, we obtain

$$J = \beta\frac{A}{2} + \frac{4}{5}Ap_{\max}R. \quad (76)$$

Inserting Eq. (76) into Eq. (74) gives

$$f_{1T}^{\perp A}(\bar{x}, k_T) = \frac{m_N N_c}{2\pi\alpha_s C_F}\frac{1}{\beta+\frac{8}{5}p_{\max}R}\frac{1}{k_T^2}\int d^2b\left\{4\bar{x}p_{\max}(\underline{b})C_1 \times\left[e^{-k_T^2/Q_s^2(\underline{b})} + 2\frac{k_T^2}{Q_s^2(\underline{b})}Ei\left(-\frac{k_T^2}{Q_s^2(\underline{b})}\right)\right] + \alpha_s\beta m_N C_2 e^{-k_T^2/Q_s^2(\underline{b})}\right\}. \quad (77)$$

Equation (77) is our final expression for the Sivers function of a nucleus in the quasiclassical approximation with the rigid rotator model for the nucleus and k_T not too much larger than Q_s. Analyzing this expression, we see that the OAM term (the first term in the curly brackets) does change sign as a function of k_T, while the Sivers density term [the second term in the curly brackets of Eq. (77)] is positive definite. Still, the first term in the curly brackets is positive for most of the k_T domain, in agreement with the qualitative argument in the Introduction corresponding to quarks being produced preferentially into the page in Fig. 2.

To study the $k_T \gg Q_s$ case, we have to return to Eq. (69): this time, we do not neglect the logarithms. A large-k_T limit implies that $|\underline{x}-\underline{y}|$ is small, and we need to expand the exponential in Eq. (70) to the lowest nontrivial (contributing) order in each term in Eq. (69). For the Sivers density term, this corresponds to replacing the exponent with 1. The remaining evaluation is easier to carry out in Eq. (67), which yields an intuitively clear formula

$$Jf_{1T}^{\perp A}(\bar{x}, k_T)|_{\text{transversity channel}, k_T\gg Q_s} = ASf_{1T}^{\perp N}(\bar{x}, k_T). \quad (78)$$

In the first term in the curly brackets of Eq. (69), we need to expand the exponential in $S_{\underline{x}\,\underline{y}}[+\infty, b^-]$ one step further, obtaining after some straightforward algebra for the whole SIDIS Sivers function

$$f_{1T}^{\perp A}(\bar{x}, k_T)\Big|_{k_T\gg Q_s} = \frac{S}{J}\left[-\frac{4\alpha_s m_N\bar{x}C_1}{3\beta k_T^6}\ln\frac{k_T^2}{\Lambda^2}\int d^2bT(\underline{b})p_{\max}(\underline{b})Q_s^2(\underline{b}) + Af_{1T}^{\perp N}(\bar{x}, k_T)\right] = \frac{\beta}{\beta+\frac{8}{5}p_{\max}R}\left[-\frac{4\alpha_s m_N\bar{x}C_1}{3\beta k_T^6}\ln\frac{k_T^2}{\Lambda^2}\int d^2bT(\underline{b})p_{\max}(\underline{b})Q_s^2(\underline{b}) + \frac{A\alpha_s^2 m_N^2 C_2}{k_T^4}\ln\frac{k_T^2}{\Lambda^2}\right]. \quad (79)$$

Since

$$\int d^2bT(\underline{b}) = A, \tag{80}$$

we see that the OAM channel contribution in Eq. (79) (the first term) is proportional to $A\alpha_s m_N p_T Q_s^2/k_T^6$, while the transversity channel contribution (the second term) scales as $A\alpha_s^2 m_N^2/k_T^4$. [Note that $x = \mathcal{O}(1)$, such that powers of x do not generate suppression.] Assuming that $p_T \approx m_N$ [see the discussion following Eq. (56)], we observe that the ratio of the OAM to the transversity channel contributions is $\sim Q_s^2/(\alpha_s k_T^2)$. [Note that for $p_T \approx m_N$, the prefactor of Eq. (79) gives a factor $\sim 1/(m_N R) \approx A^{-1/3}$ multiplying both terms, but not affecting their ratio.] We conclude that the OAM channel dominates for

$$k_T < \frac{Q_s}{\sqrt{\alpha_s}}, \tag{81}$$

that is both inside the saturation region and in a sector of phase space outside that region. For $k_T > Q_s/\sqrt{\alpha_s}$, the transversity channel dominates, mapping onto the expected perturbative QCD result [Eq. (78)].

While the main aim of this calculation is to model a nucleon at high energies, a few comments are in order about the application of this rigid rotator toy model to a realistic nucleus. Certainly a classical rigid rotator is a poor model for a real nucleus; a better approach would be to use our general result in Eq. (57) with the Wigner distribution $W(p, b)$ given by the realistic single-particle wave functions taken from nuclear structure calculations. In such realistic cases, the total angular momentum J of the nucleus is typically small, and the fraction β that comes from the nucleons' spins is also small due to nucleon spin pairing. If one were to approximate a real nucleus with this rigid rotator toy model, appropriately small J and β would need to be used in Eqs. (77) and (79). The smallness of the total OAM J does not affect the Sivers function $f_{1T}^{\perp A}$, because the magnitude is contained in the prefactor $\hat{z} \cdot (\underline{J} \times \underline{k})$ and cancels in the S/J ratio. The smallness of the spin contribution $\beta \sim \mathcal{O}(1/A)$, however, would suppress the transversity channel and ensure the dominance of the OAM term. But regardless of its applicability to a real nucleus, the rigid rotator toy model illustrates the ability of this formalism to capture the interplay of spin and angular momentum in a dense system at high energy.

IV. DRELL-YAN PROCESS

We now wish to perform a similar analysis for the Drell-Yan process $\bar{q} + A^\uparrow \to \gamma^* + X \to \ell^+\ell^- + X$, where the antiquark from the unpolarized hadron scatters on the transversely polarized hadron/nucleus, producing a spacelike photon which later decays into a dilepton pair. The annihilation subprocess $\bar{q} + q^\uparrow \to \gamma^* + X$ is related to the SIDIS process by time reversal, which leads to the famous prediction [11] that the Sivers functions entering observables in the two processes should have equal magnitudes and opposite signs.

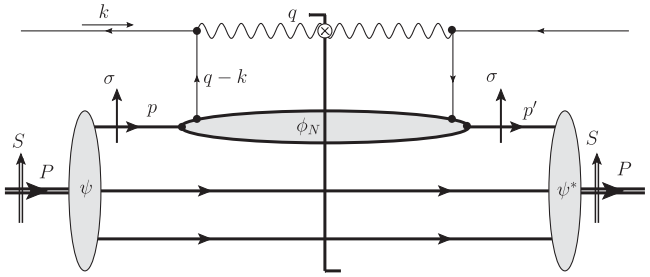

FIG. 9. Lowest-order DY process in the usual α_s power counting. An antiquark from a projectile hadron annihilates with a quark from a nucleon in the target nucleus, producing a highly virtual photon which then decays into a dilepton pair (not shown).

The lowest-order Drell-Yan annihilation process is shown in Fig. 9, without including initial-state rescattering of the antiquark on nuclear spectators. Labeling the momenta as in Fig. 9 and following along the same lines as for SIDIS, we can write the kinematics in the $\bar{q} + A^\uparrow$ center-of-mass frame as

$$\begin{aligned} P^\mu &= (P^+, M_A^2/P^+, \underline{0}), \\ p^\mu &= (p^+, (p_T^2 + m_N^2)/p^+, \underline{p}), \\ k^\mu &= \left(\frac{m_q^2}{Q^2} q^+, k^- \approx q^-, \underline{0}\right), \\ q^\mu &= (q^+, q^- \approx Q^2/q^+, \underline{q}), \end{aligned} \tag{82}$$

where

$$\begin{aligned} \hat{s} &\equiv (p+k)^2 \approx p^+ q^-, \\ x &\equiv \frac{Q^2}{2p\cdot q} \approx \frac{Q^2}{\hat{s}} \approx \frac{q^+}{p^+}. \end{aligned} \tag{83}$$

As with SIDIS, we are working in the kinematic limit $s_A = (P+k)^2 \gg \hat{s}, Q^2 \gg \perp^2$, with $\alpha \equiv p^+/P^+ \approx \hat{s}/s_A \sim \mathcal{O}(1/A)$. Again, we can compare the coherence lengths $\ell_k^- \sim 1/k^+$ of the antiquark and $\ell_\gamma^- \sim 1/q^+$ of the virtual photon

$$\begin{aligned} \frac{\ell_k^-}{L^-} &\sim \frac{1}{x}\left(\frac{Q^2}{m_q^2}\right)\frac{1}{\alpha M_A R} \sim \mathcal{O}\left(\frac{Q^2}{m_q^2} A^{-1/3}\right) \gg 1, \\ \frac{\ell_\gamma^-}{L^-} &\sim \frac{1}{x}\frac{1}{\alpha M_A R} \sim \mathcal{O}(A^{-1/3}) \ll 1. \end{aligned} \tag{84}$$

Analogous to SIDIS, this shows that the coherence length of the incoming antiquark is large; in fact, it would be infinite if we dropped the quark mass m_q as we have elsewhere in the calculation. We conclude that the long-lived antiquark is able to rescatter off of many nucleons before it finally annihilates a quark. The annihilation occurs locally, as indicated by the short coherence length of the virtual photon, and thereafter the produced photon/dilepton system does not rescatter hadronically. This again motivates the resummation of these initial state rescatterings into a Wilson-line dipole trace.

A. Quasiclassical Sivers function in DY

The entire Drell-Yan (DY) process in the quasiclassical approximation is shown in Fig. 10 at the level of the scattering amplitude: the incoming antiquark coherently scatters on the nucleons in the transversely polarized nucleus, until the last interaction in which the virtual photon is produced, which later generates the dilepton pair.[7]

By analogy with Eq. (36) in SIDIS, we write the following relation for the quark correlators in DY:

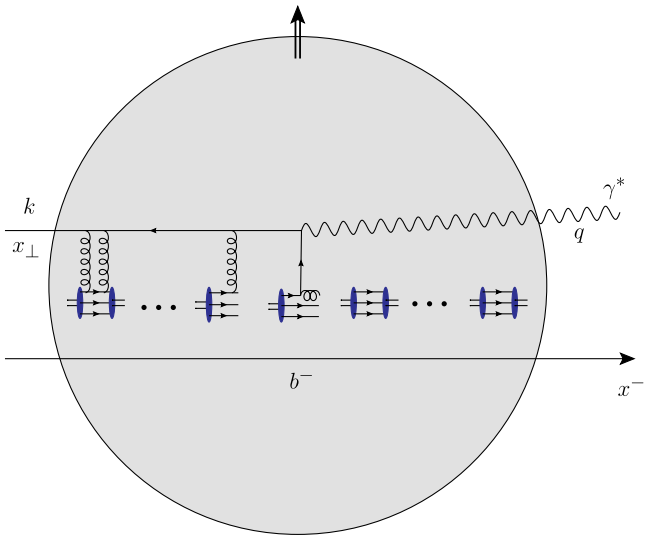

FIG. 10 (color online). Space-time structure of the quasiclassical DY process in the rest frame of the nucleus, overlaid with one of the corresponding Feynman diagrams. The shaded circle is the transversely polarized nucleus, with the vertical double arrow denoting the spin direction.

$$\mathrm{Tr}[\Phi_A(\bar{x},\underline{q};P,J)\gamma^+] = A\int\frac{dp^+d^2pdb^-}{2(2\pi)^3}\int\frac{d^2k'd^2xd^2y}{(2\pi)^2}e^{ik'\cdot(\underline{x}-\underline{y})} \times\sum_\sigma W_N^\sigma\left(p,b^-,\frac{\underline{x}+\underline{y}}{2}\right)\mathrm{Tr}[\phi_N(x,\underline{q}-\underline{k}'-x\underline{p};p,\sigma)\gamma^+]D_{\underline{y}\,\underline{x}}[b^-,-\infty], \tag{85}$$

where

$$D_{\underline{y}\,\underline{x}}[b^-,-\infty] = \left\langle\frac{1}{N_c}\mathrm{Tr}[V_{\underline{y}}[b^-,-\infty]V^\dagger_{\underline{x}}[b^-,-\infty]]\right\rangle, \tag{86}$$

and the quark correlators are defined by equations similar to (37) and (38), but now using a different gauge link [Eq. (5)]:

$$\Phi^A_{ij}(\bar{x},\underline{k};P,J) \equiv \int\frac{dx^-d^2x_\perp}{2(2\pi)^3}e^{i(\frac{1}{2}\bar{x}P^+x^- - \underline{x}\cdot\underline{k})}\langle A;P,J|\bar{\psi}_j(0)\mathcal{U}^{\mathrm{DY}}\psi_i(x^+=0,x^-,\underline{x})|A;P,J\rangle, \tag{87}$$

$$\phi^N_{ij}(x,\underline{k};p,\sigma) \equiv \int\frac{dx^-d^2x_\perp}{2(2\pi)^3}e^{i(\frac{1}{2}xp^+x^- - \underline{x}\cdot\underline{k})}\langle N;p,\sigma|\bar{\psi}_j(0)\mathcal{U}^{\mathrm{DY}}\psi_i(x^+=0,x^-,\underline{x})|N;p,\sigma\rangle. \tag{88}$$

Here $\bar{x} = Aq^+/P^+$. Equation (85) is illustrated in Fig. 11. The main difference compared to Eq. (36) is that now $\underline{k}=0$ and $\underline{q}\neq 0$.

Projecting out the DY Sivers function of the nucleus $f_{1T}^{\perp A}$ using Eq. (41) gives

$$\hat{z}\cdot(\underline{J}\times\underline{q})f_{1T}^{\perp A}(\bar{x},q_T) = \frac{M_A A}{4}\int\frac{dp^+d^2pdb^-}{2(2\pi)^3}\int\frac{d^2k'd^2xd^2y}{(2\pi)^2}e^{ik'\cdot(\underline{x}-\underline{y})}\sum_\sigma W_N^\sigma\left(p,b^-,\frac{\underline{x}+\underline{y}}{2}\right) \times\mathrm{Tr}[\phi_N(x,\underline{q}-\underline{k}'-x\underline{p};p,\sigma)\gamma^+]D_{\underline{y}\,\underline{x}}[b^-,-\infty] - (\underline{q}\to-\underline{q}). \tag{89}$$

[7]Just like for SIDIS, in small-x physics the DY process is dominated by the $\bar{q}+A\to\gamma^*+\bar{q}+A$ scattering [64], which is $\mathcal{O}(\alpha_s)$ subleading compared to the diagram in Fig. 10: since in our calculation $x=\mathcal{O}(1)$, we will neglect the $\bar{q}+A\to\gamma^*+\bar{q}+A$ process here as an $\mathcal{O}(\alpha_s)$ correction.

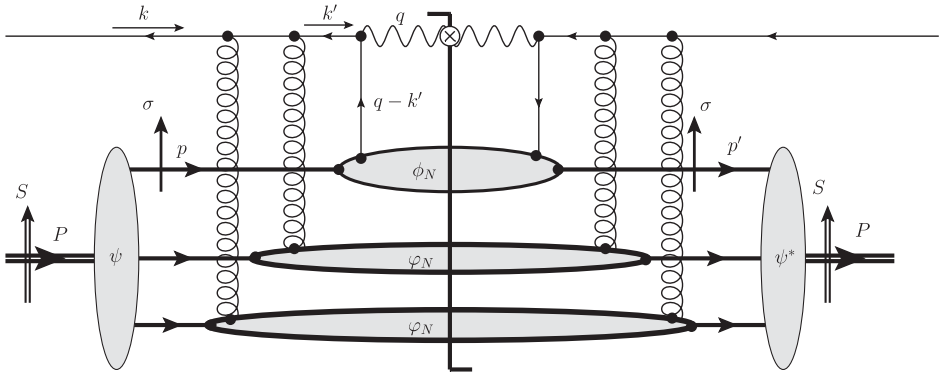

FIG. 11. Decomposition of the nuclear quark distribution Φ_A probed by the DY process into mean-field wave functions ψ, ψ^* of nucleons and the quark and gluon distributions ϕ_N and ϕ_N of the nucleons.

With the help of Eq. (40b), we write

$$\hat{z}\cdot(\underline{J}\times\underline{q})f_{1T}^{\perp A}(\bar{x},q_T)=\frac{M_A A}{2}\int\frac{dp^+d^2pdb^-}{2(2\pi)^3}\int\frac{d^2k'd^2xd^2y}{(2\pi)^2}e^{i\underline{k}'\cdot(\underline{x}-\underline{y})}\sum_\sigma W_N^\sigma\left(p,b^-,\frac{\underline{x}+\underline{y}}{2}\right)$$
$$\times\left[f_1^N(x,|\underline{q}-\underline{k}'-x\underline{p}|_T)+\frac{1}{m_N}\hat{z}\cdot(\underline{\sigma}\times(\underline{q}-\underline{k}'-x\underline{p}))f_{1T}^{\perp N}(x,|\underline{q}-\underline{k}'-x\underline{p}|_T)\right]$$
$$\times D_{\underline{y}\,\underline{x}}[b^-,-\infty]-(\underline{q}\to-\underline{q}). \tag{90}$$

Performing the spin sums [Eq. (44)] gives

$$\hat{z}\cdot(\underline{J}\times\underline{q})f_{1T}^{\perp A}(\bar{x},q_T)=\frac{M_A}{2}\int\frac{dp^+d^2pdb^-}{2(2\pi)^3}\int\frac{d^2k'd^2xd^2y}{(2\pi)^2}e^{i\underline{k}'\cdot(\underline{x}-\underline{y})}\left[AW_{\rm unp}\left(p,b^-,\frac{\underline{x}+\underline{y}}{2}\right)\right.$$
$$\times f_1^N(x,|\underline{q}-\underline{k}'-x\underline{p}|_T)+W_{\rm trans}\left(p,b^-,\frac{\underline{x}+\underline{y}}{2}\right)\frac{1}{m_N}\hat{z}\cdot(\underline{S}\times(\underline{q}-\underline{k}'-x\underline{p}))$$
$$\left.\times f_{1T}^{\perp N}(x,|\underline{q}-\underline{k}'-x\underline{p}|_T)\right]D_{\underline{y}\,\underline{x}}[b^-,-\infty]-(\underline{q}\to-\underline{q}). \tag{91}$$

In the terms being subtracted in Eq. (91) with $(\underline{q}\to-\underline{q})$, we can also reverse the dummy integration variables $\underline{k}'\to-\underline{k}'$, $\underline{p}\to-\underline{p}$, and $\underline{x}\leftrightarrow\underline{y}$. This leaves the Fourier factor and the distributions f_1^N, $f_{1T}^{\perp N}$ invariant, giving

$$\hat{z}\cdot(\underline{J}\times\underline{q})f_{1T}^{\perp A}(\bar{x},q_T)=\frac{M_A}{2}\int\frac{dp^+d^2pdb^-}{2(2\pi)^3}\int\frac{d^2k'd^2xd^2y}{(2\pi)^2}e^{i\underline{k}'\cdot(\underline{x}-\underline{y})}\left\{f_1^N(x,|\underline{q}-\underline{k}'-x\underline{p}|_T)\right.$$
$$\times A\left[W_{\rm unp}\left(p^+,\underline{p},b^-,\frac{\underline{x}+\underline{y}}{2}\right)D_{\underline{y}\,\underline{x}}[b^-,-\infty]-W_{\rm unp}\left(p^+,-\underline{p},b^-,\frac{\underline{x}+\underline{y}}{2}\right)D_{\underline{x}\,\underline{y}}[b^-,-\infty]\right]$$
$$+\frac{1}{m_N}\hat{z}\cdot(\underline{S}\times(\underline{q}-\underline{k}'-x\underline{p}))f_{1T}^{\perp N}(x,|\underline{q}-\underline{k}'-x\underline{p}|_T)$$
$$\left.\times\left[W_{\rm trans}\left(p^+,\underline{p},b^-,\frac{\underline{x}+\underline{y}}{2}\right)D_{\underline{y}\,\underline{x}}[b^-,-\infty]+W_{\rm trans}\left(p^+,-\underline{p},b^-,\frac{\underline{x}+\underline{y}}{2}\right)D_{\underline{x}\,\underline{y}}[b^-,-\infty]\right]\right\}. \tag{92}$$

We recognize the factors in brackets from the SIDIS case [Eq. (50)], rewriting Eq. (92) as

$$\hat{z}\cdot(\underline{J}\times\underline{q})f_{1T}^{\perp A}(\bar{x},q_T)=M_A\int\frac{dp^+d^2pdb^-}{2(2\pi)^3}\int\frac{d^2k'd^2xd^2y}{(2\pi)^2}e^{i\underline{k}'\cdot(\underline{x}-\underline{y})}\Bigg\{f_1^N(x,|\underline{q}-\underline{k}'-x\underline{p}|_T)$$
$$\times A\left[W_{\rm unp}^{\rm OAM}\left(p^+,\underline{p},b^-,\frac{\underline{x}+\underline{y}}{2}\right)S_{\underline{y}\,\underline{x}}[b^-,-\infty]+W_{\rm unp}^{\rm symm}\left(p^+,\underline{p},b^-,\frac{\underline{x}+\underline{y}}{2}\right)iO_{\underline{y}\,\underline{x}}[b^-,-\infty]\right]$$
$$+\frac{1}{m_N}\hat{z}\cdot(\underline{S}\times(\underline{q}-\underline{k}'-x\underline{p}))f_{1T}^{\perp N}(x,|\underline{q}-\underline{k}'-x\underline{p}|_T)$$
$$\times\left[W_{\rm trans}^{\rm symm}\left(p^+,\underline{p},b^-,\frac{\underline{x}+\underline{y}}{2}\right)S_{\underline{y}\,\underline{x}}[b^-,-\infty]+W_{\rm trans}^{\rm OAM}\left(p^+,\underline{p},b^-,\frac{\underline{x}+\underline{y}}{2}\right)iO_{\underline{y}\,\underline{x}}[b^-,-\infty]\right]\Bigg\}. \quad (93)$$

As before, we drop contributions from the odderon $iO_{\underline{y}\,\underline{x}}$ as being outside the precision of the quasiclassical formula [Eq. (85)] to get

$$\hat{z}\cdot(\underline{J}\times\underline{q})f_{1T}^{\perp A}(\bar{x},q_T)=M_A\int\frac{dp^+d^2pdb^-}{2(2\pi)^3}\int\frac{d^2k'd^2xd^2y}{(2\pi)^2}e^{i\underline{k}'\cdot(\underline{x}-\underline{y})}\Bigg\{AW_{\rm unp}^{\rm OAM}\left(p^+,\underline{p},b^-,\frac{\underline{x}+\underline{y}}{2}\right)$$
$$\times f_1^N(x,|\underline{q}-\underline{k}'-x\underline{p}|_T)+\frac{1}{m_N}\hat{z}\cdot(\underline{S}\times(\underline{q}-\underline{k}'-x\underline{p}))W_{\rm trans}^{\rm symm}\left(p^+,\underline{p},b^-,\frac{\underline{x}+\underline{y}}{2}\right)$$
$$\times f_{1T}^{\perp N}(x,|\underline{q}-\underline{k}'-x\underline{p}|_T)\Bigg\}S_{\underline{y}\,\underline{x}}[b^-,-\infty]. \quad (94)$$

Since the rotational momentum of the nucleons p_T is assumed to be small, we have to expand in it to the lowest nontrivial order. Shifting the integration variable $\underline{k}'\to\underline{k}'+\underline{q}-x\underline{p}$ in Eq. (94) and expanding the exponential to the lowest nontrivial order in p_T, we obtain [cf. Eq. (57)]

$$\hat{z}\cdot(\underline{J}\times\underline{q})f_{1T}^{\perp A}(\bar{x},q_T)=M_A\int\frac{dp^+d^2pdb^-}{2(2\pi)^3}\int\frac{d^2k'd^2xd^2y}{(2\pi)^2}e^{-i(\underline{q}-\underline{k}')\cdot(\underline{x}-\underline{y})}$$
$$\times\Bigg\{ix\underline{p}\cdot(\underline{x}-\underline{y})AW_{\rm unp}^{\rm OAM}\left(p^+,\underline{p},b^-,\frac{\underline{x}+\underline{y}}{2}\right)f_1^N(x,k_T')$$
$$-\frac{1}{m_N}\hat{z}\cdot(\underline{S}\times\underline{k}')W_{\rm trans}^{\rm symm}\left(p^+,\underline{p},b^-,\frac{\underline{x}+\underline{y}}{2}\right)f_{1T}^{\perp N}(x,k_T')\Bigg\}S_{\underline{x}\,\underline{y}}[b^-,-\infty], \quad (95)$$

where we have also interchanged $\underline{x}\leftrightarrow\underline{y}$ and $\underline{k}'\to-\underline{k}'$.

Equation (95) is our main formal result for the DY Sivers function. We again see that the Sivers function in DY can arise through two distinct channels in this quasiclassical approach: the OAM channel that contains its preferred direction in the distribution $W_{\rm unp}^{\rm OAM}$ and the transversity/Sivers density channel that generates its preferred direction through a local lensing mechanism $f_{1T}^{\perp N}$.

To demonstrate the importance of the Wilson lines for the Sivers function, for the moment, let us ignore the contribution of the Wilson lines associated with initial-state rescattering in Eq. (95). Without any such initial-state interactions, the nucleonic Sivers function is zero, $f_{1T}^N=0$ [21,22,48], leaving

$$\hat{z}\cdot(\underline{J}\times\underline{q})f_{1T}^{\perp A}(\bar{x},q_T)=M_A\int\frac{dp^+d^2pdb^-}{2(2\pi)^3}\int\frac{d^2k'd^2xd^2y}{(2\pi)^2}e^{-i(\underline{q}-\underline{k}')\cdot(\underline{x}-\underline{y})}$$
$$\times ix\underline{p}\cdot(\underline{x}-\underline{y})AW_{\rm unp}^{\rm OAM}\left(p^+,\underline{p},b^-,\frac{\underline{x}+\underline{y}}{2}\right)f_1^N(x,k_T')=0, \quad (96)$$

which vanishes after b^- integration because of the rotational and PT-symmetry conditions [Eq. (B7)].

B. Sign reversal of the Sivers function between SIDIS and DY

Now that the DY Sivers function [Eq. (95)] is expressed in the same form as the Sivers function for SIDIS [Eq. (57)], we can compare both expressions to see how the nuclear Sivers functions have changed between SIDIS and DY and understand the origin of the SIDIS/DY sign-flip relation [11]

$$f_{1T}^{\perp A}(x,k_T)|_{\rm SIDIS} = -f_{1T}^{\perp A}(x,k_T)|_{\rm DY}. \tag{97}$$

First, we notice that the transversity/Sivers density channel (the second term in the curly brackets) has changed signs as required between Eqs. (57) and (95). Mathematically, this occurs because of the $\underline{k}' \to -\underline{k}'$ interchange, simply because the momentum going into the Wilson line in SIDIS corresponds to the momentum coming from the Wilson line in DY (cf. Figs. 5 and 11). The transversity/Sivers density channel contribution thus automatically satisfies the sign-flip relation [Eq. (97)].

The OAM channel contribution to Eq. (95) is more subtle; although the prefactor has not changed as compared to Eq. (57), the longitudinal coordinate b^- integral entering Eq. (95) for DY can be modified using $b^- \to -b^-$ substitution along with Eq. (B7) to give

$$\int db^- W_{\rm unp}^{\rm OAM}(p,b) S_{\underline{x}\,\underline{y}}[b^-,-\infty] = -\int db^- W_{\rm unp}^{\rm OAM}(p,b) S_{\underline{x}\,\underline{y}}[-b^-,-\infty]. \tag{98}$$

When evaluating the dipole S matrix, we neglect the polarization effects as being energy suppressed. Therefore, for the purpose of this S matrix, the nucleus has a rotational symmetry around the z axis (see Fig. 6 for axis labels). We thus write

$$S_{\underline{x}\,\underline{y}}[-b^-,-\infty] \overset{PT}{=} S_{-\underline{x},-\underline{y}}[+\infty,b^-] \overset{z-\text{rotation}}{=} S_{\underline{x}\,\underline{y}}[+\infty,b^-], \tag{99}$$

where z rotation denotes a half-revolution around the z axis. Using Eq. (99) in Eq. (98), we arrive at

$$\overbrace{\int db^- W_{\rm unp}^{\rm OAM}(p,b) S_{\underline{x}\,\underline{y}}[b^-,-\infty]}^{\rm DY} = -\overbrace{\int db^- W_{\rm unp}^{\rm OAM}(p,b) S_{\underline{x}\,\underline{y}}[+\infty,b^-]}^{\rm SIDIS}. \tag{100}$$

One can also simply see that Eq. (100) is true by using the quasiclassical GM/MV dipole S matrix from Eq. (70) on its right-hand side, along with

$$S_{\underline{x}\underline{y}}[b^-,-\infty] = \exp\left[-\frac{1}{4}|\underline{x}-\underline{y}|^2 Q_s^2 \left(\frac{\underline{x}+\underline{y}}{2}\right)\left(\frac{b^-+R^-}{2R^-}\right) \ln\frac{1}{|\underline{x}-\underline{y}|\Lambda}\right] \tag{101}$$

on its left-hand side. We conclude that the OAM channel contributions to the SIDIS Sivers function [Eq. (57)] and the DY Sivers function [Eq. (95)] also satisfy the sign-flip relation [Eq. (97)].

Therefore, for any Wigner distribution $W(p,b)$, the Sivers functions at the quasiclassical level for SIDIS [Eq. (57)] and for DY [Eq. (95)] are equal in magnitude and opposite in sign [Eq. (97)]. This statement is a direct consequence of the invariance of $W(p,b)$ under rotations and PT-reversal, Eq. (B7), and it mirrors in this context the original derivation by Collins [11].

The advantage of our approach here, apart from providing the explicit formal results in Eqs. (57) and (95), is in the new physical interpretation of the transverse spin asymmetry in the OAM channel. As described in the Introduction following Fig. 1, the incoming antiquark is more likely to interact with the "front" of the nucleus due to shadowing effects, thus scattering on the nucleon moving out of the page in Fig. 1. This is justified by the $S_{\underline{x}\underline{y}}[b^-,-\infty]$ function in Eq. (95) [see also Eq. (101)], which is largest for $b^- = -R^-$. Thus, the virtual photon is produced preferentially out of the page; this leads to a nonzero STSA in DY. The sign reversal relation follows from comparing Figs. 1 and 2: in DY, the particles are produced preferentially left of beam, while in SIDIS, the produced hadrons come out mainly right of beam.

The rigid rotator toy model of Sec. III C can also be constructed for the DY Sivers function. However, due to the sign-reversal relation [Eq. (97)], we can read off the answer for the DY Sivers function in the rigid rotator model as being the negative of that in Eq. (77) for moderate k_T and the negative of Eq. (79) for $k_T \gg Q_s$. All the conclusions about the relative importance of the two contributing channels remain the same.

V. DISCUSSION

The main goal of this work was to construct SIDIS and DY Sivers functions in the quasiclassical GM/MV approximation, which models a proton as a large nucleus, and which we modified by giving the nucleus a nonzero OAM. The main formal results are given in Eqs. (57) (SIDIS) and (95) (DY). We showed that there are two main mechanisms generating the quasiclassical Sivers function: the OAM channel and the transversity channel. The former is leading in saturation power counting; it also dominates for $k_T < Q_s/\sqrt{\alpha_s}$, that is both inside and—for $Q_s < k_T < Q_s/\sqrt{\alpha_s}$—outside of the saturation region. At higher k_T, the transversity channel dominates. In the future

our quasiclassical calculation can be augmented by including evolution corrections to the Sivers function, making the whole formalism ready for phenomenological applications, similar to the successful use of nonlinear small-x evolution equations [65–71] for the description (and prediction) of high-energy scattering data [72,73].

Perhaps just as important, we constructed a novel physical mechanism of the STSA generation. This is the OAM channel. The OAM mechanism, while diagrammatically very similar to the original BHS mechanism [10], provides a different interpretation from the "lensing" effect [10,21] or the color-Lorentz force of Refs. [18,19]. The OAM mechanism is described in the Introduction, in the discussion around Figs. 1 and 2. It is based on interpreting the extra rescattering proposed by BHS as a shadowing-type correction. The STSA is then generated by the combination of the OAM and shadowing. The shadowing makes sure the projectile interacts differently with the front and the back of the target, generating the asymmetry of the produced particles.

While shadowing is a high-energy phenomenon, and our calculation was done in the high-energy approximation $\hat{s} \gg \perp^2$ [though for $x \sim \mathcal{O}(1)$], it may be that the OAM mechanism for generating STSA is still valid for lower-energy scattering, though of course the formulas derived above would not apply in such a regime. At lower energies, the difference between the interactions of the projectile with the front/back of the target may result from, say, energy loss of the projectile as it traverses the target. Again, combined with the target rotation, this would generate STSA, and hence, the Sivers function. The formalism needed to describe such a low-energy process would be quite different from the one presented above; moreover, the correct degrees of freedom may not be quarks and gluons anymore. However, the main physics principle of combining OAM with the difference in interaction probabilities between the projectile and front/back of the target to generate STSA may be valid at all energies.

Returning to higher energies and the derived formulas in Eqs. (57) and (95), let us point out that these results, when applied to experimental data, may allow one to determine the distribution of intrinsic transverse momentum $\underline{p}(\underline{b}, b^-)$ of partons in the hadronic or nuclear target, along with the transversity/Sivers function density in the target. This would complement the existing methods of spatial imaging of quarks and gluons inside the hadrons and nuclei [74], providing a new independent cross-check for those methods.

ACKNOWLEDGMENTS

We would like to thank Daniel Boer, Dick Furnstahl, Leonard Gamberg and Feng Yuan for useful correspondence. This research is sponsored in part by the U. S. Department of Energy under Grant No. DE-SC0004286.

APPENDIX A: WIGNER DISTRIBUTIONS WITH MULTIPLE RESCATTERINGS

The aim of this appendix is to justify the result given in Eq. (23). To study the interplay between the local "knock-out" channel of deep inelastic scattering and the coherent multiple rescattering on the nuclear remnants, it is illustrative to consider a minimal case with both features. This process, shown in Fig. 12, consists of the knockout subprocess followed by a single rescattering on a different quark from a second nucleon in the nucleus. Rescattering on a second nucleon receives a combinatoric enhancement of order $\sim A^{1/3}$ compared to rescattering on the same nucleon; the former is $\mathcal{O}(1)$ in the saturation power counting, while the latter is $\mathcal{O}(\alpha_s)$.

The total SIDIS amplitude $M_{\rm tot}$ depicted in Fig. 12 consists of a loop integral connecting the mean-field single-particle wave functions $\psi(p)$ of the nucleus to a scattering amplitude M_{K+R} denoting both the "knockout" and rescattering processes:

$$M_{\rm tot} = \int \frac{dr^+ d^2r}{2(2\pi)^3} \frac{P^+}{(p_1^+ - r^+)(p_2^+ + r^+)} \times \psi(p_1 - r)\psi(p_2 + r) M_{K+R}(p_1 - r, p_2 + r, q, k, r), \tag{A1}$$

where a sum over spins and colors of the participating quarks is implied. Squaring both sides of Eq. (A1) and integrating out the final-state momenta p_1 and p_2 gives

$$\begin{aligned}\langle |M_{\rm tot}|^2 \rangle &\equiv A(A-1) \int \frac{dp_1^+ d^2p_1 dp_2^+ d^2p_2}{[2(2\pi)^3]^2 (p_1^+ + q^+) p_2^+} |M_{\rm tot}|^2 \\ &= \int \frac{dp_1^+ d^2p_1 dp_2^+ d^2p_2}{[2(2\pi)^3]^2 (p_1^+ + q^+) p_2^+} \frac{dr^+ d^2r}{2(2\pi)^3} \frac{dr'^+ d^2r'}{2(2\pi)^3} \frac{A(A-1)(P^+)^2}{\sqrt{(p_1^+ - r^+)(p_2^+ + r^+)(p_1^+ - r'^+)(p_2^+ + r'^+)}} \\ &\times \int db_1^- d^2b_1 db_2^- d^2b_2 e^{-i(r-r')\cdot(b_1-b_2)} W\left(p_1 - \frac{r+r'}{2}, b_1\right) W\left(p_2 + \frac{r+r'}{2}, b_2\right) \\ &\times M_{K+R}(p_1 - r, p_2 + r, q, k, r) M^*_{K+R}(p_1 - r', p_2 + r', q, k, r'),\end{aligned} \tag{A2}$$

where we have employed the Wigner distributions defined in Eq. (16) above and summed over all pairs of nucleons.

Equation (A2) is still far from Eq. (23), because in Eq. (A2) we do not have the amplitude squared: instead, we have the product of M_{K+R} and M^*_{K+R} with different arguments. It is easier to further analyze the expression separately for the transverse and longitudinal degrees of freedom. We proceed by taking the classical limits, in which case the Wigner distributions give us the position and momentum distributions of nucleons simultaneously. Moreover, for the large nucleus at hand, the Wigner distributions depend on $\underline{b}_1$ and $\underline{b}_2$ weakly over the perturbatively short distances associated with the Feynman diagrams. We thus define $\underline{b} = (\underline{b}_1 + \underline{b}_2)/2$ and $\underline{\Delta}b = \underline{b}_1 - \underline{b}_2$ and write

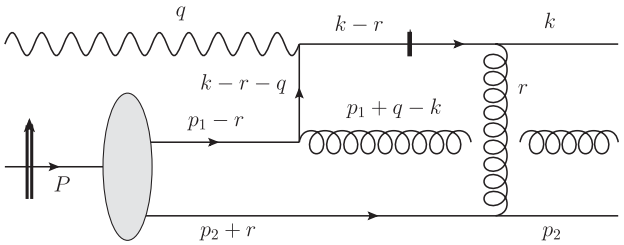

FIG. 12. The minimal SIDIS process containing both the "knockout" of a quark from the nuclear wave function and rescattering on a different quark from a second nucleon. The short, thick vertical line indicates that the pole of the intermediate quark propagator is picked up in the calculation.

$$\begin{aligned}
&\int d^2r d^2r' d^2b_1 d^2b_2 e^{i(\underline{r}-\underline{r}')\cdot(\underline{b}_1-\underline{b}_2)} W\left(p_1 - \frac{r+r'}{2}, b_1\right) W\left(p_2 + \frac{r+r'}{2}, b_2\right) \\
&\times M_{K+R}(p_1 - r, p_2 + r, q, k, r) M^*_{K+R}(p_1 - r', p_2 + r', q, k, r') \approx \int d^2r d^2r' d^2b d^2\Delta b e^{i(\underline{r}-\underline{r}')\cdot\underline{\Delta}b} \\
&\times W\left(p_1 - \frac{r+r'}{2}, b_1^-, \underline{b}\right) W\left(p_2 + \frac{r+r'}{2}, b_2^-, \underline{b}\right) M_{K+R}(p_1 - r, p_2 + r, q, k, r) \\
&\times M^*_{K+R}(p_1 - r', p_2 + r', q, k, r') = (2\pi)^2 \int d^2r d^2b W\left(p_1^+ - \frac{r^+ + r'^+}{2}, \underline{p}_1 - \underline{r}, b_1^-, \underline{b}\right) \\
&\times W\left(p_2^+ + \frac{r^+ + r'^+}{2}, \underline{p}_2 + \underline{r}, b_2^-, \underline{b}\right) M_{K+R}(p_1^+ - r^+, \underline{p}_1 - \underline{r}, p_2^+ + r^+, \underline{p}_2 + \underline{r}, q, k, r^+, \underline{r}) \\
&\times M^*_{K+R}(p_1^+ - r'^+, \underline{p}_1 - \underline{r}, p_2^+ + r'^+, \underline{p}_2 + \underline{r}, q, k, r'^+, \underline{r}).
\end{aligned} \tag{A3}$$

Now the difference in the arguments of M_{K+R} and M^*_{K+R} is only in the longitudinal momenta r^+ and r'^+. To integrate over these momenta we notice that, as follows from Fig. 12, in the high-energy kinematics at hand, the leading contribution to the amplitude M_{K+R} comes from the region where $p_1^+, p_2^+ \gg r^+, r'^+$. In this regime we combine Eqs. (A2) and (A3) to write

$$\begin{aligned}
\langle |M_{\rm tot}|^2 \rangle = &\int \frac{dp_1^+ d^2p_1 dp_2^+ d^2p_2}{[2(2\pi)^3]^2 (p_1^+ + q^+) p_2^+} \frac{dr^+ dr'^+ d^2r}{4(2\pi)^4} \frac{(P^+)^2}{p_1^+ p_2^+} db_1^- db_2^- d^2b e^{-i\frac{1}{2}(r^+ - r'^+)(b_1^- - b_2^-)} A(A-1) \\
&\times W(p_1^+, \underline{p}_1 - \underline{r}, b_1^-, \underline{b}) W(p_2^+, \underline{p}_2 + \underline{r}, b_2^-, \underline{b}) M_{K+R}(p_1^+, \underline{p}_1 - \underline{r}, p_2^+, \underline{p}_2 + \underline{r}, q, k, r^+, \underline{r}) \\
&\times M^*_{K+R}(p_1^+, \underline{p}_1 - \underline{r}, p_2^+, \underline{p}_2 + \underline{r}, q, k, r'^+, \underline{r}).
\end{aligned} \tag{A4}$$

In the $p_1^+, p_2^+ \gg r^+, r'^+$ kinematics, the amplitude M_{K+R} contains only one pole in r^+ resulting from the denominator of the $k - r$ quark propagator (cf. Refs. [25,33,63]). We can thus write

$$M_{K+R}(p_1 - r, p_2 + r, q, k) = \frac{i}{(k-r)^2 + i\varepsilon} \tilde{M}_{K+R}(p_1 - r, p_2 + r, q, k), \tag{A5}$$

where $\tilde{M}_{K+R}$ denotes the rest of the diagram which does not contain singularities in r^+ in the $p_1^+, p_2^+ \gg r^+, r'^+$ approximation. (Note that $\tilde{M}_{K+R}$ also contains the numerator of the $k - r$ quark propagator.) Since $(k-r)^2 \approx -k^- r^+ + \underline{k}^2 - (\underline{k} - \underline{r})^2$, we can use Eq. (A5) to integrate over r^+:

$$\int_{-\infty}^{\infty}\frac{dr^+}{2\pi}e^{-i\frac{1}{2}r^+(b_1^- - b_2^-)}M_{K+R}(p_1-r,p_2+r,q,k)$$
$$\approx\frac{1}{k^-}\theta(b_2^- - b_1^-)\tilde{M}_{K+R}(p_1^+,\underline{p}_1-\underline{r},p_2^+,\underline{p}_2+\underline{r},q,k)$$
$$=\frac{1}{k^-}\theta(b_2^- - b_1^-)M_K(p_1-r,q,k-r)M_R(p_2+r,k-r,k,r). \tag{A6}$$

Here we assume that $r^+ = [\underline{k}^2 - (\underline{k}-\underline{r})^2]/k^- \approx 0$ in our kinematics. After putting the $k-r$ quark propagator on mass shell, the amplitude $\tilde{M}_{K+R}$ factorizes into a product of separate amplitudes for knockout $M_K(p_1-r,q,k-r)$ and rescattering $M_R(p_2+r,k-r,k,r)$ [25,33,63], as employed in Eq. (A6), where the sum over quark polarizations and colors is implicit.

With the help of Eq. (A6) (and a similar one for the r'^+ integration of M^*_{K+R}), we write

$$\langle|M_{\rm tot}|^2\rangle = \int\frac{dp_1^+d^2p_1dp_2^+d^2p_2}{[2(2\pi)^3]^2(p_1^+ + q^+)p_2^+}\frac{d^2r}{4(2\pi)^2}\frac{A(A-1)(P^+)^2}{p_1^+p_2^+(k^-)^2}db_1^-db_2^-d^2b\theta(b_1^- - b_2^-)$$
$$\times W(p_1^+,\underline{p}_1-\underline{r},b_1^-,\underline{b})W(p_2^+,\underline{p}_2+\underline{r},b_2^-,\underline{b})$$
$$\times|M_K(p_1-r,q,k-r)|^2|M_R(p_2+r,k-r,k,r)|^2. \tag{A7}$$

Defining the energy-independent (at the quasiclassical level) rescattering amplitude by [25,33]

$$|A_R(p_2+r,k-r,k,r)|^2 \equiv \frac{1}{4(p_2^+)^2(k^-)^2}|M_R(p_2+r,k-r,k,r)|^2 \tag{A8}$$

and denoting the average of this object in the Wigner distribution by the angle brackets,

$$\langle|A_R(k,r)|^2\rangle(b_1^-,\underline{b}) = \int\frac{dp_2^+d^2p_2db_2^-}{2(2\pi)^3}\theta(b_2^- - b_1^-)(A-1)W(p_2^+,\underline{p}_2+\underline{r},b_2^-,\underline{b})\times|A_R(p_2+r,k-r,k,r)|^2, \tag{A9}$$

we rewrite Eq. (A7) as

$$\langle|M_{\rm tot}|^2\rangle = A\int\frac{dp_1^+d^2p_1db_1^-d^2b}{2(2\pi)^3}\frac{(P^+)^2}{p_1^+(p_1^+ + q^+)}W(p_1^+,\underline{p}_1,b_1^-,\underline{b})$$
$$\times\int\frac{d^2r}{(2\pi)^2}|M_K(p_1,q,k-r)|^2\langle|A_R(k,r)|^2\rangle(b_1^-,\underline{b}). \tag{A10}$$

In arriving at Eq. (A10), we have shifted the momentum $p_1 \to p_1 + r$.

We now define the "energy-independent" total and "knockout" amplitudes [25,33]

$$|A_{\rm tot}|^2 \equiv \frac{1}{4(P^+)^2(q^-)^2}|M_{\rm tot}|^2, \qquad |A_k|^2 \equiv \frac{1}{4(p_1^+)^2(q^-)^2}|M_K|^2. \tag{A11}$$

Employing the Fourier transform [Eq. (21)], we reduce Eq. (A10) to

$$\langle|A_{\rm tot}|^2\rangle = A\int\frac{dp_1^+d^2p_1db_1^-d^2b}{2(2\pi)^3}\frac{p_1^+}{p_1^+ + q^+}W(p_1^+,\underline{p}_1,b_1^-,\underline{b})\int d^2xd^2ye^{-i\underline{k}\cdot(\underline{x}-\underline{y})}$$
$$\times A_K(p_1,q,k^-,r^+,\underline{x}-\underline{b})A_K^*(p_1,q,k^-,r^+,\underline{y}-\underline{b})\langle|A_R|^2\rangle(k^-,\underline{x}-\underline{y},b_1^-,\underline{b}) \tag{A12}$$

with

$$\langle|A_R|^2\rangle(k^-,\underline{x}-\underline{y},b_1^-,\underline{b}) = \int\frac{d^2r}{(2\pi)^2}e^{i\underline{r}\cdot(\underline{x}-\underline{y})}\langle|A_R(k,r)|^2\rangle(b_1^-,\underline{b}). \tag{A13}$$

Comparing Eq. (A10) to Eq. (22), we see that, just like in all high-energy QCD scattering calculations [25,30–33], the rescattering can be factored out into a multiplicative factor in the transverse coordinate space. Similar to the above, one can show that all further rescatterings would only introduce more multiplicative factors. Defining a somewhat abbreviated notation

$$A(p,q,\underline{x}-\underline{b})A^*(p,q,\underline{y}-\underline{b}) \equiv A_K(p,q,k^-,r^+,\underline{x}-\underline{b})A_K^*(p,q,k^-,r^+,\underline{y}-\underline{b}) \times \langle |A_R|^2\rangle(k^-,\underline{x}-\underline{y},b_1^-,\underline{b}), \tag{A14}$$

we see that Eq. (A12) reduces to Eq. (23), as desired. The above discussion also demonstrates how multiple rescatterings factorize in the transverse coordinate space: in the high-energy kinematics, they are included through the Wilson lines of Eqs. (26) and (27). The Wilson-line correlator $D_{\underline{xy}}[+\infty,b^-]$ from Eq. (27) contains a b^--ordered product of multiple rescattering factors $\langle |A_R|^2\rangle$ from all the interacting nucleons [63,75].

APPENDIX B: THE ROLE OF *PT* SYMMETRY

The decompositions in Eqs. (57) and (95) essentially break the Wilson-line operator $\mathcal{U}$ in definition (2) into two parts: the coherent rescattering $S_{\underline{xy}}[+\infty,b^-]$ on other spectator nucleons, which is a leading-order contribution in the saturation power counting; and the subleading lensing interaction with the same nucleon, which generates $f_{1T}^{\perp N}$. If we neglect the Wilson-line operator $\mathcal{U}$ entirely, then we know that the Sivers function of the nucleus $f_{1T}^{\perp A}$ must vanish, as first proved by Collins [15]. But if we drop $f_{1T}^{\perp N}$ and $S_{\underline{xy}}[+\infty,b^-]$ from Eq. (57), we do not obviously get zero:

$$\hat{z}\cdot(\underline{J}\times\underline{k})f_{1T}^{\perp A}(x,k_T) = M_A A\int\frac{dp^+d^2pdb^-}{2(2\pi)^3}d^2xd^2y\frac{d^2k'}{(2\pi)^2}e^{-i(\underline{k}-\underline{k}')\cdot(\underline{x}-\underline{y})} \times ix\underline{p}\cdot(\underline{x}-\underline{y})W_{\rm unp}^{\rm OAM}\left(p^+,\underline{p},b^-,\frac{\underline{x}+\underline{y}}{2}\right)f_1^N(x,k_T')\overset{?}{=}0. \tag{B1}$$

The right-hand side of this equation must vanish for wave functions described by $W_{\rm unp}^{\rm OAM}$ that are *PT* eigenstates [15]; we can see this explicitly by considering the constraints on $W_\sigma(p,b)$ due to rotational invariance and *PT* symmetry. It is most convenient to enumerate the rotational symmetry properties of the nucleon distribution $W_\sigma(p,b)$ in the rest frame of the nucleus, using a cylindrical vector basis coaxial to the transverse spin vector $\underline{S}$. This basis $(\hat{e}_\rho,\hat{e}_\theta,\hat{x})$ is shown in Fig. 13 and is defined by

$$\begin{pmatrix}\hat{e}_\rho\\ \hat{e}_\theta\end{pmatrix} = \begin{pmatrix} b_y/b_\rho & b_z/b_\rho \\ -b_z/b_\rho & b_y/b_\rho\end{pmatrix}\begin{pmatrix}\hat{y}\\ \hat{z}\end{pmatrix} = \begin{pmatrix}\cos\theta & \sin\theta\\ -\sin\theta & \cos\theta\end{pmatrix}\begin{pmatrix}\hat{y}\\ \hat{z}\end{pmatrix}, \tag{B2}$$

where $(p_\rho(b),p_\theta(b)) = p\cdot(\hat{e}_\rho(b),\hat{e}_\theta(b))$ and $b_\rho \equiv \sqrt{b_y^2+b_z^2}$.

First, the distribution must be symmetric under rotations about the transverse spin S_x, which are easy to express in this cylindrical basis:

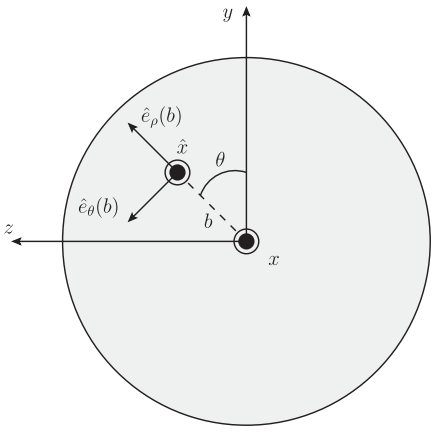

FIG. 13. Definition of the cylindrical coordinate basis [Eq. (B2)] convenient for formulating the symmetry properties of the nucleonic distribution $W_\sigma(p,b)$ in the rest frame of the nucleus.

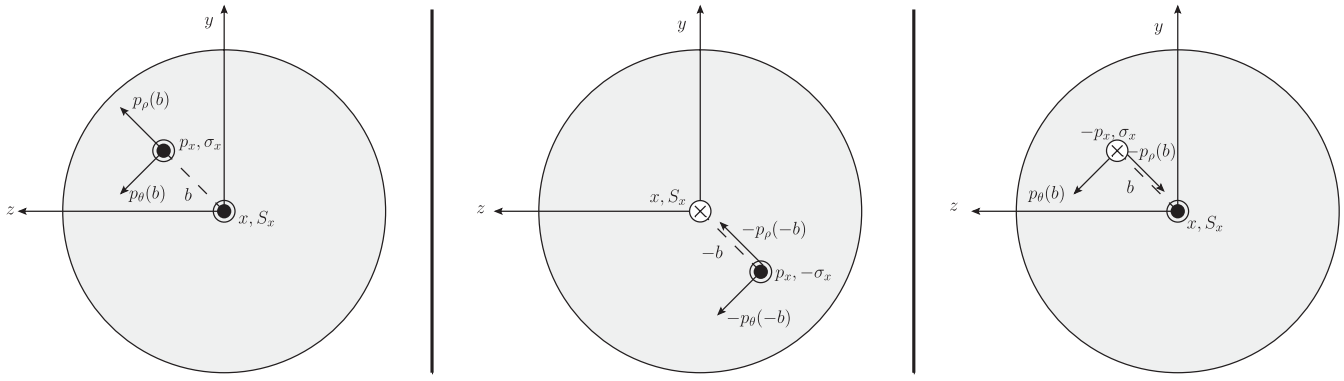

FIG. 14. Illustration of the *PT* transformation and rotational symmetry in the rest frame used in Eq. (B4). Left panel: Illustration of the momentum flow represented by $W_\sigma(p,b)$. Center panel: Under a *PT* transformation, the spins S,σ and coordinate b are reversed, but the momentum p is invariant. Right panel: Rotation of the center panel by π about the vector $\vec{S}\times\vec{b}$ returns the distribution to its original position b, with p_ρ and p_x having been reversed.

$$W_\sigma(p_x; p_\rho(b); p_\theta(b); b) = W_\sigma(p_x; p_\rho(b'); p_\theta(b'); b'). \tag{B3}$$

Second, if the nucleus is in a PT-symmetric eigenstate of the QCD Hamiltonian, then $W_\sigma(p, b)$ should be invariant under PT transformations. These transformations reverse the coordinates $(b \to -b)$ and pseudovectors like the spin $(S, \sigma \to -S, -\sigma)$ but leave the momentum vector p unchanged. Using this transformation, together with rotational invariance as shown in Fig. 14, we obtain

$$\begin{aligned} W_\sigma(p_\rho(b), p_\theta(b), p_x; b; S_x) &\overset{PT}{=} W_{-\sigma}(p_\rho(b), p_\theta(b), p_x; -b; -S_x) \\ &= W_{-\sigma}(-p_\rho(-b), -p_\theta(-b), p_x; b; -S_x) \\ &\overset{R_b}{=} W_\sigma(-p_\rho(b), p_\theta(b), -p_x; b; S_x) \\ &\therefore \\ W_\sigma(p_\rho(b), p_\theta(b), p_x; b; S_x) &= W_\sigma(-p_\rho(b), p_\theta(b), -p_x; b; S_x), \end{aligned} \tag{B4}$$

where the rotation R_b is a half-revolution in the Sb plane. This means that in a PT eigenstate with transverse spin S_x, the only allowed direction of net momentum flow corresponds to the azimuthal orbital momentum p_θ and explains the naming convention W^{OAM} in Eq. (49).

The distributions that enter Eqs. (57) and (95), however, are the (anti)symmetrized distributions under reversal of the transverse momenta $(p_x, p_y \to -p_x, -p_y)$. For these purposes, it is more convenient to write the distribution $W_\sigma(p, b)$ in terms of the Cartesian basis:

$$W(p_x, p_y, p_z; b) = W_\sigma\left(p_x; \frac{b_y}{b_\rho} p_\rho(b) - \frac{b_z}{b_\rho} p_\theta(b); \frac{b_z}{b_\rho} p_\rho(b) + \frac{b_y}{b_\rho} p_\theta(b); b\right). \tag{B5}$$

Using the symmetry properties [Eqs. (B3) and (B4)], we can write the $\underline{p}$-reversed distribution in terms of the distribution at a point $\bar{b} \equiv (b_x, b_y, -b_z)$ on the opposite side of the nucleus:

$$\begin{aligned} W_\sigma(-p_x, -p_y, p_z; b) &= W_\sigma\left(-p_x; -\frac{b_y}{b_\rho} p_\rho(b) + \frac{b_z}{b_\rho} p_\theta(b); \frac{b_z}{b_\rho} p_\rho(b) + \frac{b_y}{b_\rho} p_\theta(b); b\right) \\ &\overset{\text{Eq.(B3)}}{=} W_\sigma\left(-p_x; -\frac{b_y}{b_\rho} p_\rho(\bar{b}) - \frac{b_z}{b_\rho} p_\theta(\bar{b}); -\frac{b_z}{b_\rho} p_\rho(\bar{b}) + \frac{b_y}{b_\rho} p_\theta(\bar{b}); \bar{b}\right) \\ &\overset{\text{Eq.(B4)}}{=} W_\sigma\left(p_x; \frac{b_y}{b_\rho} p_\rho(\bar{b}) - \frac{b_z}{b_\rho} p_\theta(\bar{b}); \frac{b_z}{b_\rho} p_\rho(\bar{b}) + \frac{b_y}{b_\rho} p_\theta(\bar{b}); \bar{b}\right) \\ &= W_\sigma(p_x, p_y, p_z; \bar{b}) \\ &\therefore \\ W_\sigma(-p_x, -p_y, p_z; b) &= W_\sigma(p_x, p_y, p_z; \bar{b}). \end{aligned} \tag{B6}$$

Thus, a nucleon on the back side of the nucleus has an opposite transverse momentum to a corresponding nucleon in the front of the nucleus. Therefore, the (anti)symmetrized distributions have definite parity under $b_z \to -b_z$:

$$\begin{aligned} W_\sigma^{\mathrm{symm}}(p, b) &\equiv \frac{1}{2}[W_\sigma(p, b) + (\underline{p} \to -\underline{p})] = +W_\sigma^{\mathrm{symm}}(p, \bar{b}), \\ W_\sigma^{\mathrm{OAM}}(p, b) &\equiv \frac{1}{2}[W_\sigma(p, b) - (\underline{p} \to -\underline{p})] = -W_\sigma^{\mathrm{OAM}}(p, \bar{b}). \end{aligned} \tag{B7}$$

Equation (B7) tells us that a consequence of PT invariance in the nucleus is that the orbital angular momentum encountered at any point in the front of the nucleus is compensated by an equal and opposite orbital angular momentum from a corresponding point on the back of the nucleus. This is the resolution to the apparent paradox in Eq. (B1): when we neglect all Wilson-line contributions (both $S_{\underline{xy}}[+\infty, b^-]$ and $f_{1T}^{\perp N}$), the net

asymmetry in the quark distribution is zero, since $\int db^- W^{\mathrm{OAM}}_{\mathrm{unp}}(p,b) = 0$. Hence, neglecting all Wilson-line contributions yields a zero Sivers function, consistent with Ref. [15].

An essential role is played in Eq. (57), then, by the rescattering factor $S_{\underline{xy}}[+\infty, b^-]$. In the OAM channel, even though the rescattering $S_{\underline{xy}}[+\infty, b^-]$ is not the source of a preferred transverse direction, without it the net contribution to the Sivers function from OAM would vanish after integration over b^-, as can be gleaned from the left panel in Fig. 7. The rescattering factor $S_{\underline{xy}}[+\infty, b^-]$ is essential because it introduces shadowing that breaks this front-back symmetry by screening quarks ejected from the front of the nucleus more than those ejected from the back. The Sivers function relevant for SIDIS is therefore more sensitive to OAM from the back of the nucleus than from the front, which prevents the complete cancellation of the OAM contribution as in Eq. (B1).

This analysis is strikingly similar to the arguments that historically established the existence of the Sivers function. As Collins argued in Ref. [15], *PT* invariance of any hadronic eigenstate prohibits a preferred direction that can generate the Sivers function. This is directly reflected in the vanishing of Eq. (B1) without the effects of multiple rescattering. And as Brodsky, Hwang, and Schmidt demonstrated in Ref. [10], the rescattering represented by the semi-infinite Wilson lines breaks this symmetry and permits a preferred direction for the asymmetry. Unlike that calculation, however, here the rescattering does not occur as color-correlated "lensing" due to rescattering on the remnants of the active quark. Here the interaction is explicitly color decorrelated because the rescattering occurs on many nucleons whose colors are not correlated. Despite this difference, the rescattering effects are still sufficient to break the front-back symmetry and give rise to a net preferred direction for the asymmetry.

[1] J. C. Collins, D. E. Soper, and G. F. Sterman, Adv. Ser. Dir. High Energy Phys. **5**, 1 (1988).
[2] J. C. Collins and D. E. Soper, Nucl. Phys. **B193**, 381 (1981).
[3] D. W. Sivers, Phys. Rev. D **41**, 83 (1990).
[4] D. W. Sivers, Phys. Rev. D **43**, 261 (1991).
[5] A. Efremov and O. Teryaev, Sov. J. Nucl. Phys. **36**, 140 (1982).
[6] A. Efremov and O. Teryaev, Phys. Lett. **150B**, 383 (1985).
[7] J.-w. Qiu and G. F. Sterman, Phys. Rev. Lett. **67**, 2264 (1991).
[8] X.-D. Ji, Phys. Lett. B **289**, 137 (1992).
[9] J.-w. Qiu and G. F. Sterman, Phys. Rev. D **59**, 014004 (1998).
[10] S. J. Brodsky, D. S. Hwang, and I. Schmidt, Phys. Lett. B **530**, 99 (2002).
[11] J. C. Collins, Phys. Lett. B **536**, 43 (2002).
[12] Y. Koike and S. Yoshida, Phys. Rev. D **84**, 014026 (2011).
[13] Y. Kanazawa and Y. Koike, Phys. Lett. B **478**, 121 (2000).
[14] Y. Kanazawa and Y. Koike, Phys. Lett. B **490**, 99 (2000).
[15] J. C. Collins, Nucl. Phys. **B396**, 161 (1993).
[16] G. L. Kane, J. Pumplin, and W. Repko, Phys. Rev. Lett. **41**, 1689 (1978).
[17] Y. V. Kovchegov and M. D. Sievert, Phys. Rev. D **86**, 034028 (2012).
[18] M. Burkardt, arXiv:0810.3589.
[19] M. Burkardt, *Proc. Sci.*, LC2010 (**2010**) 051.
[20] A. V. Belitsky, X. Ji, and F. Yuan, Nucl. Phys. **B656**, 165 (2003).
[21] S. J. Brodsky, D. S. Hwang, Y. V. Kovchegov, I. Schmidt, and M. D. Sievert, Phys. Rev. D **88**, 014032 (2013).
[22] S. J. Brodsky, D. S. Hwang, and I. Schmidt, Nucl. Phys. **B642**, 344 (2002).
[23] L. Gamberg and M. Schlegel, AIP Conf. Proc. **1374**, 309 (2011).
[24] L. Gamberg and M. Schlegel, Phys. Lett. B **685**, 95 (2010).
[25] A. H. Mueller, Nucl. Phys. **B335**, 115 (1990).
[26] L. D. McLerran and R. Venugopalan, Phys. Rev. D **49**, 3352 (1994).
[27] L. D. McLerran and R. Venugopalan, Phys. Rev. D **50**, 2225 (1994).
[28] L. D. McLerran and R. Venugopalan, Phys. Rev. D **49**, 2233 (1994).
[29] E. Iancu and R. Venugopalan, arXiv:hep-ph/0303204.
[30] H. Weigert, Prog. Part. Nucl. Phys. **55**, 461 (2005).
[31] J. Jalilian-Marian and Y. V. Kovchegov, Prog. Part. Nucl. Phys. **56**, 104 (2006).
[32] F. Gelis, E. Iancu, J. Jalilian-Marian, and R. Venugopalan, Annu. Rev. Nucl. Part. Sci. **60**, 463 (2010).
[33] Y. V. Kovchegov and E. Levin, *Quantum Chromodynamics at High Energy* (Cambridge University Press, Cambridge, 2012).
[34] Y. V. Kovchegov, Phys. Rev. D **55**, 5445 (1997).
[35] D. Boer, A. Dumitru, and A. Hayashigaki, Phys. Rev. D **74**, 074018 (2006).
[36] D. Boer, A. Utermann, and E. Wessels, Phys. Lett. B **671**, 91 (2009).
[37] D. Boer and A. Dumitru, Phys. Lett. B **556**, 33 (2003).
[38] F. Dominguez, J.-W. Qiu, B.-W. Xiao, and F. Yuan, Phys. Rev. D **85**, 045003 (2012).
[39] A. Metz and J. Zhou, Phys. Rev. D **84**, 051503 (2011).
[40] Z.-B. Kang and F. Yuan, Phys. Rev. D **84**, 034019 (2011).
[41] Z.-B. Kang and B.-W. Xiao, Phys. Rev. D **87**, 034038 (2013).

[42] K. Golec-Biernat and M. Wüsthoff, Phys. Rev. D **59**, 014017 (1998).
[43] K. Golec-Biernat and M. Wüsthoff, Phys. Rev. D **60**, 114023 (1999).
[44] H. Kowalski and D. Teaney, Phys. Rev. D **68**, 114005 (2003).
[45] P. Tribedy and R. Venugopalan, Nucl. Phys. **A850**, 136 (2011).
[46] T. Chou and C. N. Yang, Nucl. Phys. **B107**, 1 (1976).
[47] D. Boer, L. Gamberg, B. Musch, and A. Prokudin, J. High Energy Phys. 10 (2011) 021.
[48] D. Boer, S. J. Brodsky, and D. S. Hwang, Phys. Rev. D **67**, 054003 (2003).
[49] D. Boer and P. Mulders, Phys. Rev. D **57**, 5780 (1998).
[50] G. P. Lepage and S. J. Brodsky, Phys. Rev. D **22**, 2157 (1980).
[51] S. J. Brodsky, G. P. Lepage, and P. B. Mackenzie, Phys. Rev. D **28**, 228 (1983).
[52] L. Łukaszuk and B. Nicolescu, Lett. Nuovo Cimento **8**, 405 (1973).
[53] B. Nicolescu, contribution to the Moriond 1990 Conference.
[54] C. Ewerz, arXiv:hep-ph/0306137.
[55] J. Bartels, L. Lipatov, and G. Vacca, Phys. Lett. B **477**, 178 (2000).
[56] Y. V. Kovchegov, L. Szymanowski, and S. Wallon, Phys. Lett. B **586**, 267 (2004).
[57] Y. Hatta, E. Iancu, K. Itakura, and L. McLerran, Nucl. Phys. **A760**, 172 (2005).
[58] A. Kovner and M. Lublinsky, J. High Energy Phys. 02 (2007) 058.
[59] S. Jeon and R. Venugopalan, Phys. Rev. D **71**, 125003 (2005).
[60] A. Bacchetta, M. Boglione, A. Henneman, and P. Mulders, Phys. Rev. Lett. **85**, 712 (2000).
[61] A. Bacchetta and P. Mulders, Phys. Rev. D **62**, 114004 (2000).
[62] K. Itakura, Y. V. Kovchegov, L. McLerran, and D. Teaney, Nucl. Phys. **A730**, 160 (2004).
[63] Y. V. Kovchegov and A. H. Mueller, Nucl. Phys. **B529**, 451 (1998).
[64] B. Kopeliovich, J. Raufeisen, A. Tarasov, and M. Johnson, Phys. Rev. C **67**, 014903 (2003).
[65] I. Balitsky, Nucl. Phys. **B463**, 99 (1996).
[66] Y. V. Kovchegov, Phys. Rev. D **60**, 034008 (1999).
[67] J. Jalilian-Marian, A. Kovner, and H. Weigert, Phys. Rev. D **59**, 014015 (1998).
[68] E. Iancu, A. Leonidov, and L. D. McLerran, Nucl. Phys. **A692**, 583 (2001).
[69] I. I. Balitsky, Phys. Rev. D **75**, 014001 (2007).
[70] E. Gardi, J. Kuokkanen, K. Rummukainen, and H. Weigert, Nucl. Phys. **A784**, 282 (2007).
[71] Y. Kovchegov and H. Weigert, Nucl. Phys. **A784**, 188 (2007).
[72] J. L. Albacete, N. Armesto, J. G. Milhano, P. Quiroga-Arias, and C. A. Salgado, Eur. Phys. J. C **71**, 1705 (2011).
[73] J. L. Albacete and A. Dumitru, arXiv:1011.5161.
[74] A. Accardi, J. Albacete, M. Anselmino, N. Armesto, E. Aschenauer *et al.*, arXiv:1212.1701.
[75] J. Jalilian-Marian, A. Kovner, L. D. McLerran, and H. Weigert, Phys. Rev. D **55**, 5414 (1997).